2018

An Automated Analysis Of Single Particle Tracking Data For Proteins That Exhibit Multi Component Motion.

Rehan Ali
University of Vermont

AN AUTOMATED ANALYSIS OF SINGLE PARTICLE TRACKING DATA FOR PROTIENS THAT EXHIBIT MULTI COMPONENT MOTION.

A Thesis Presented

by

Rehan Ali

to

The Faculty of the Graduate College

of

The University of Vermont

In Partial Fulfillment of the Requirements
for the Degree of Master of Science
Specializing in Neuroscience

May, 2018

Defense Date: March 29, 2018
Thesis Examination Committee:

Anthony Morielli, Advisor
Jason Stumpff, Chairperson
Christopher L Berger, Ph.D.
Cynthia J. Forehand, Ph.D., Dean of the Graduate College

ABSTRACT

Neurons are polarized cells with dendrites and an axon projecting from their cell body. Due to this polarized structure a major challenge for neurons is the transport of material to and from the cell body. The transport that occurs between the cell body and axons is called Axonal transport. Axonal transport has three major components: molecular motors which act as vehicles, microtubules which serve as tracks on which these motors move and microtubule associated proteins which regulate the transport of material. Axonal transport maintains the integrity of a neuron and its dysfunction is linked to neurodegenerative diseases such as, Alzheimer's disease, Frontotemporal dementia linked to chromosome 17 and Pick's disease. Therefore, understanding the process of axonal transport is extremely important.

Single particle tracking is one method in which axonal transport is studied. This involves fluorescent labelling of molecular motors and microtubule associated proteins and tracking their position in time. Single particle tracking has shown that both, molecular motors and microtubule associated proteins exhibit motion with multiple components. These components are directed, where motion is in one direction, diffusive, where motion is random, and static, where there is no motion. Moreover, molecular motors and microtubule associated proteins also switch between these different components in a single instance of motion.

We have developed a MATLAB program, called MixMAs, which specializes in analyzing the data provided by single particle tracking. MixMAs uses a sliding window approach to analyze trajectories of motion. It is capable of distinguishing between different components of motion that are exhibited by molecular motors and microtubule associated proteins. It also identifies transitions that take place between different components of motion. Most importantly, it is not limited by the number of transitions and the number of components present in a single trajectory. The analysis results provided by MixMAs include all the necessary parameters required for a complete characterization of a particle's motion. These parameters are the number of different transitions that take place between different components of motion, the dwell times of different components of motion, velocity for directed component of motion and diffusion coefficient for diffusive component of motion.

We have validated the working of MixMAs by simulating motion of particles which show all three components of motion with all the possible transitions that can take place between them. The simulations are performed for different values of error in localizing the position of a particle. The simulations confirm that MixMAs accurately calculates parameters of motion for a range of localization errors. Finally, we show an application of MixMAs on experimentally obtained single particle data of Kinesin-3 motor.

ACKNOWLEDGEMENTS

Firstly, I thank Dr. Christopher L Berger for his immense support and excellent mentorship during my study here. Everything that has been accomplished in this thesis wouldn't have been possible without him. I would like to thank him and his family who invited me to their annual thanksgiving dinner every year. I also thank all the members of the Berger lab especially Jamie Stern, for her helpful suggestions, Lynn Chrin, for taking care of laboratory business so that all members of the Berger lab could concentrate on their research, Dominique Lessard, for providing the data for Kinesin-3 which is used in this study, and Gregory Hoeprich (former lab member) for listening to numerous ideas that I had and providing suggestions on how to implement them.

Additionally, I thank Dr. Jason Stumpff for his invaluable suggestions and for allowing me the use of microscope of the Stumpff lab. I also thank him for his help in setting up the dynamic microtubule assay. I also thank Cindy Fonseca for conversations that would turn a depressing day into a happy one. I also thank Heidi Malaby for all the walks that we took with our dogs.

I would also like to specially appreciate Carrie Perkins for her guidance and support during my stay here, especially when I needed such support the most. I also thank Dean Forehand for helping me in completing my studies by providing guidance and taking care of official business at the graduate college so that I did not have to worry about filling and submitting numerous forms.

Lastly, and most importantly, I than Dr. Anthony Morielli for taking me under his mentorship at a time when I need a mentor exactly like him. Not only did he become a great mentor for me, but also without his proofreading of this thesis and his corrections and suggestions this work couldn't have been completed.

I also thank my dog, Hani, for forcing me take her for walks as many ideas that have been used in this thesis came to my mind when I was thinking about this work during those walks.

TABLE OF CONTENTS

LIST OF FIGURES

CHAPTER 1: INTRODUCTION

1.1. Summary

A major challenge for neurons is transport of material from the cell body to the axon terminal and vice versa. Understanding the process of axonal transport will not only enhance our knowledge of neurons but it is crucial for understanding the pathology of neurodegenerative diseases associated with disruptions in axonal transport, such as Alzheimer's Disease (AD), Frontotemporal Dementia Linked to Chromosome 17 (FTDP) and Pick's disease (Connell et al., 2001; Barghorn et al., 2004; Bunker et al., 2006a; LeBoeuf et al., 2008a; Smith et al., 2009; Iyer et al., 2013; Gatchel et al., 2017).

The basic machinery of axonal transport involves movement of proteins along microtubules. This process involves numerous tubulin interacting proteins, including Microtubules Associated Proteins (MAPs) and cytoskeletal motors (Maday et al., 2014). Understanding the properties of their motion along microtubules provides a fundamental foundation for understanding axonal transport in general.

Advances in protein labelling (Adams et al., 2002; Andresen et al., 2004; Chen et al., 2005; DeRocco et al., 2010; Campos et al., 2011; Benke et al., 2012; Shank et al., 2013; Raeisolsadati Oskouei and Brouwer, 2017), fluorescent microscopy (Thompson and Lagerholm, 1997; Pierce and Vale, 1999; Gustafsson, 2000; Schmoranzer et al., 2000; Toomre and Manstein, 2001; Betzig et al., 2006; Willig et al., 2006b; Willig et al., 2006a; Kellner et al., 2007; Willig et al., 2007; Schermelleh et al., 2008) and computational approaches to particle tracking techniques (Sage et al., 2005; Jaqaman et al., 2008; Ram et al., 2008; Ruhnow et al., 2011; Liu et al., 2013; Chaphalkar et al., 2016; Mangeol et al., 2016; Xiao et al., 2016) provide the essential technical means to experimentally study

protein movement along microtubules in great detail. Using Single Particle Tracking (SPT) a term that defines the entire experimental process, from labelling to tracking particles in images, the function of MAPs such as Tau and molecular motors such as Kinesin-3 is being investigated. But there is a limited availability of tools specialized for analyzing data gathered using SPT (Heaslip et al., 2014; Chaphalkar et al., 2016; Mangeol et al., 2016). These tools are also limited to analyzing SPT data when particle trajectories have no transitions from one component to another (Chaphalkar et al., 2016; Mangeol et al., 2016), or only have a single transition (Heaslip et al., 2014). To fill this gap, we have developed a MATLAB (MathWorks, Natick, 2015) program that is specifically designed to analyze SPT data in which particle trajectories can have multiple components of motion with multiple transitions between these components.

In the following section, a literature review of axonal transport and its major components; microtubules, Tau and molecular motors will be presented. The need for the current study in the context of investigations that are using SPT will be presented in section 2.1 of chapter 2.

1.2. Axonal transport

1.2.1. A summary of neuron structure and its role in the nervous system

Neurons, the basic information processing units of the nervous system, consist of a cell body with processes emanating from it. One of these processes is called a dendrite. A neuron can have a variable number of dendrites depending on its type. Dendrites receive signals from other neurons and electrically transmit these signals to the cell body of the neuron. The cell body then performs summation of these signals and then sends a signal to the axon, a long single process emanating from the cell body of the neuron. Signal form

the cell body is sent by initiating an action potential at the axon initial segment (AIS). This signal, then in the form of an axon potential, moves towards the axon terminal. Here numerous processes can occur. For example, for a motor neuron the signal will cause some motor activity. In another example, if the axon terminal makes a synapse with dendrites of one or more neurons it will initiate activity in those neurons (Kandel, 1995; Lodish H, 2000). This example implies that neurons can be linked together with one or more neurons receiving a signal and transmitting it to the connected neurons which then produce an output.

A collection of neurons linked together form a neural network (Reece, 2011) capable of performing computations much like a computer program where an input is received and an output is generated. In the case of a neural network the input is a stimulus and the output is a decision which alters some physiological or cognitive function. The human brain can be regarded as a collection of many neural networks linked to each other forming a supra neural network controlling physical and cognitive functions

1.2.2. Axonal transport: its need and its major components

The need for axonal transport

A problem for neurons, that arises due to their polarized structure (Kandel, 1995; Lodish H, 2000; Reece, 2011) is the transport of proteins that are required in certain distant regions but are synthesized in the cell body. Considering that axon lengths can vary from a range of millimeters to meters, the transport of material from the cell body to the axon and vice versa is a major challenge for proper functioning of neurons (Maday et al., 2014).

Major components of axonal transport

The process of transport of material from the cell body to axons and vice versa is termed as axonal transport. In axonal transport a cargo, the material to be transported, binds to a motor protein. The motor protein can also bind microtubules, which serve as tracks for the motor protein's motion. The motor protein with the cargo, then moves along the microtubule in a directional manner (Hirokawa, 1998). The direction in which a motor protein moves depends on the motor's type. A family of motor proteins called Kinesin (Vale et al., 1985), with a few exceptions, transports cargo towards the axon terminal (Okada et al., 1995). Another family of proteins called Dynein transports cargo towards the cell body (Schnapp and Reese, 1989).

Apart from microtubules and motor proteins, MAPs are also an important component of axonal transport as they regulate the transport of material. This regulation can be achieved in numerous ways which include, altering microtubule structure, preventing motor proteins binding to the microtubule, regulating microtubule dynamics and altering motor protein's motion along the microtubule (Amos and Schlieper, 2005).

In summary, the major components of axonal transport include microtubules, motors proteins and MAPs (Figure 1). Therefore, a comprehensive study of axonal transport requires a comprehensive study of these components. The study of these components is also necessary because, as mentioned before, dysfunction of axonal transport is implicated in Alzheimer's disease, FTDP-17 and numerous other neurodegenerative diseases (Connell et al., 2001; Barghorn et al., 2004; Bunker et al., 2006a; LeBoeuf et al., 2008a; Smith et al., 2009; Iyer et al., 2013; Gatchel et al., 2017).

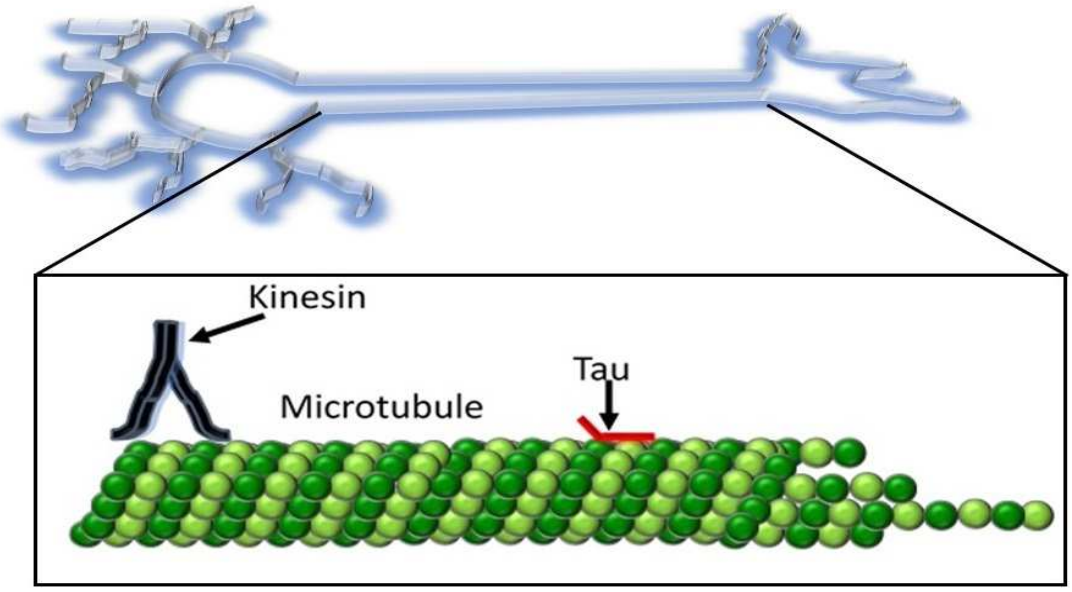

Figure 1: Axonal transport components: Microtubules act as tracks on which Kinesin motors move cargo and Tau regulates axonal transport

1.3. Microtubules serve as tracks for axonal transport

1.3.1. Microtubule structure

Microtubules are polymers composed of tubulin dimers (Figure 2). A tubulin dimer consists of α-tubulin and β-tubulin. In a microtubule these dimers interact longitudinally in an end to end fashion with α-tubulin of one dimer interacting with β-tubulin of another dimer (Amos and Klug, 1974). Interaction in this fashion results in a single polar filament, called a protofilament, with α-tubulin at one end (referred to as the minus end) and β-tubulin at the other end (referred to as the plus end) (Amos and Baker, 1979). A number of these protofilaments, usually 13 (Tilney et al., 1973; Jones, 1975), interact laterally (Henderson and Unwin, 1975), with a vertical off set of 3 monomers between 2 laterally interacting filaments, to form, an approximately 25 nm in diameter, a hollow helical structure called microtubule. As all laterally interacting protofilaments have

their plus ends at one end of the microtubule and their minus ends are at the other end of the microtubule, the microtubule also become a polar structure with a minus and a plus end (Jones, 1975; Beese et al., 1987; Nogales et al., 1999; Song et al., 2013). This polarity has physiological consequences because, in axons microtubules are arranged with their minus ends towards the cell body and their plus ends towards the axon terminal (Baas et al., 1988). This arrangement is important because, as mentioned before, motor proteins, show specificity in the direction in which they move along a microtubule (Schnapp and Reese, 1989; Okada et al., 1995; Hirokawa, 1998).

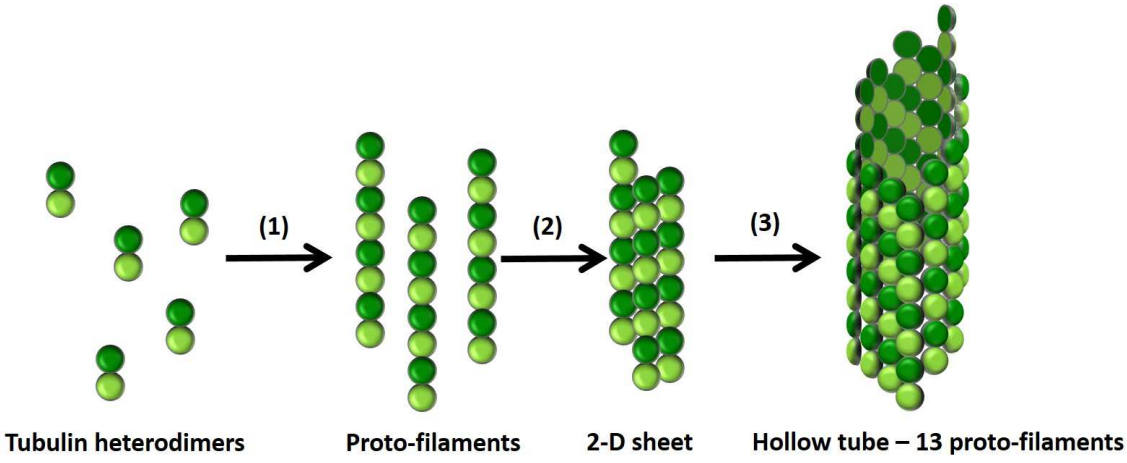

Figure 2: Microtubule structure: (1) Tubulin heterodimers interact longitudinally to form proto-filaments. (2) Proto-filaments interact laterally to form a 2-D sheet. (3) The 2-D sheet closes to form a hollow structure of 13 proto-filaments called microtubule.

1.3.2. Microtubule formation

Formation of microtubules is a 2-stage process. The first stage is called nucleation in which tubulin dimers interact to form a structure from which a microtubule will be polymerized (Zheng et al., 1995; Oakley et al., 2015; Sulimenko et al., 2017). Tubulin dimers are GTPases, which incorporate into the microtubule lattice in a Guanosine-tri-

phosphate (GTP) bound state where it is hydrolyzed to Guanosine-di GDP (Hyman et al., 1992; Chen and Doxsey, 2012). *In vitro,* a high concentration of tubulin and an excess of GTP means that nucleation does not require additional proteins, whereas *in vivo,* microtubule nucleation occurs from structures, composed of different proteins, called Microtubule Organizing Centers (MTOC) (Zheng et al., 1995; Oakley et al., 2015; Sulimenko et al., 2017). Nucleation stage results in the formation of a seed from which a microtubule can polymerize.

The second stage in the formation of microtubules is the polymerization stage. In this stage GTP incorporated tubulin dimers are added to the ends of the microtubules. This addition of dimers occurs at both the minus and the plus end of a microtubule but the rate of addition of dimers at the plus end is much higher than the rate of addition of tubulin dimers at the minus end. Therefore, the growth velocity of a microtubule at the plus end is much higher than the growth velocity of the microtubule at the minus end (Walker et al., 1988; Stewart et al., 1990; Kerssemakers et al., 2006).

1.3.3. Dynamic instability of microtubules; Description and importance

The discussion so far has focused on the structure, formation and growth of microtubules but microtubules are dynamic polymers. What that means is that they can alternate between a polymerization phase, where tubulin dimers are added to the ends of microtubules resulting in growth of a microtubule, and a depolymerization phase, where tubulin dimers leave the ends of microtubules resulting in shortening of a microtubule. This dynamic behavior of microtubules is termed as dynamic instability (Mitchison and Kirschner, 1984; Gardner et al., 2013; Li et al., 2014) (Figure 3). To characterize the dynamic instability of a microtubule the following parameters need to be calculated: The

growth velocity in the polymerization phase (this is usually measured for the plus end of a microtubule), the shortening velocity (this too is usually measured for the plus end of a microtubule), the frequency of transitions from the growth phase to the shortening phase (this transition is called a catastrophe) and the frequency of transitions from the shortening phase to the growth phase (this transition is called a rescue) (Mitchison and Kirschner, 1984; Gardner et al., 2013; Li et al., 2014).

A complete characterization of microtubule dynamic instability is an important scientific goal since dynamic instability behavior of microtubules is crucial for numerous cellular processes. Axonal transport requires proper regulation of microtubule dynamics, as dysfunction of MAPs which regulate microtubule dynamics, is linked to neurodegenerative disorders (Goedert et al., 1998; Henriques et al., 2010; Gauthier-Kemper et al., 2011; Cartelli et al., 2016). Microtubule dynamics also needs to be tightly regulated for the formation of growth cones (Kempf et al., 1996) and axonal regeneration (Ruschel et al., 2015).

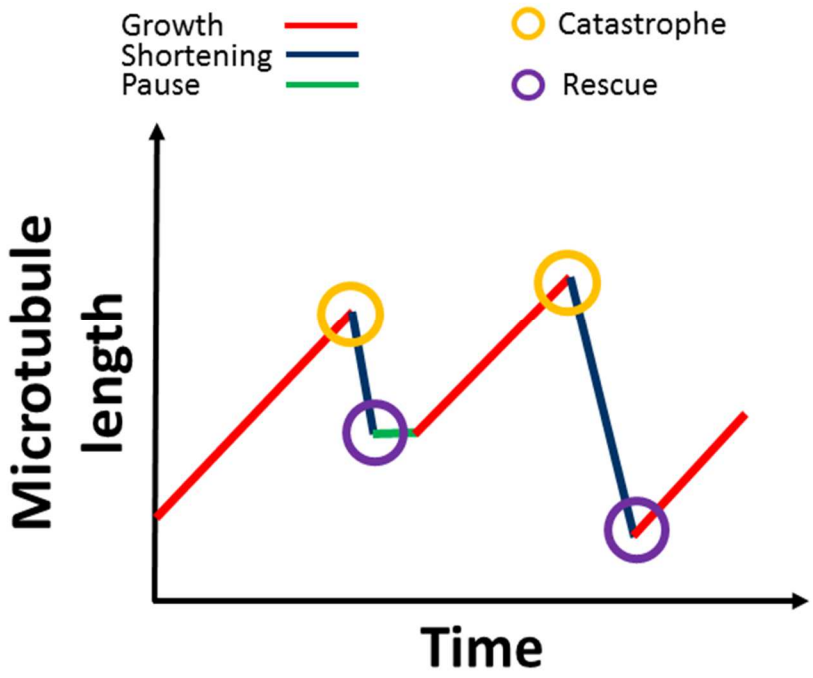

Figure 3: Microtubule dynamic instability: Microtubule length shown as a function of time.

1.4. Tau regulates axonal transport

1.4.1. Tau isoforms and its primary structure

Tau is a MAP expressed mainly in neurons and localized mainly in axons. It performs a wide range of functions including regulation of axonal transport, and regulation of development of polarity in neurons. Tau has also been shown to be involved in numerous other important physiological processes. Tau's dysfunction is linked to numerous diseases including Alzheimer's disease, FTDP-17, Pick's disease and progressive supra nuclear palsy (Brandt et al., 2005; Cowan and Mudher, 2013; Wang et al., 2013).

Six major isoforms of Tau are expressed in the adult human brain (Goedert and Jakes, 1990). These isoforms differ in their primary structures (Figure 4). Near the carboxy-terminus of Tau protein there are tandem repeats which form a part of the region called,

the Microtubule binding domain (Gustke et al., 1994). These repeats are variable in isoforms leading to Tau isoforms division into two classes; 1- Isoforms with three microtubule binding repeats (3R) and 2- Isoforms with four microtubule binding repeats (4R). Another variable region in the primary structure of Tau is near the amino-terminus of the protein, where there are a variable number of 29 amino acid long acidic inserts. An isoform of Tau, within each class (based on the number of microtubule binding repeats), can either have zero (S), one (M) or two (L) amino-terminal acidic inserts (Gustke et al., 1994). In this way the six isoforms can be defined as 3RS, 3RM, 3RL, 4RS, 4RM and 4RL. These six isoforms range from 352 to 441 amino acids in length and from 48 to 67 Kilo Daltons in molecular weight. (Goedert and Jakes, 1990; Gustke et al., 1994).

(a)

(b)

Alternatively spliced regions	3RS	3RM	3RL	4RS	4RM	4RL
N1	Absent	Present	Present	Absent	Present	Present
N2	Absent	Absent	Present	Absent	Absent	Present
R2	Absent	Absent	Absent	Present	Present	Present

Figure 4: (a) Schematic of the primary structure of the longest isoform of Tau (4RL). (b) Table illustrating the differences in the primary structure of the six isoforms of Tau.

1.4.2. Tau regulates microtubule dynamics

Tau regulates microtubule dynamics and numerous studies emphasizing Tau's physiological importance have focused on this function of Tau. Methods used to study microtubule dynamics include light scattering assays, direct observation using dark field

microscopy and direct observation using total internal reflection (TIRF) microscopy. The prevailing consensus is that Tau 'stabilizes' microtubules. But, as some conflicting results have been obtained from different studies and the term 'stability' has been used in different contexts in different studies, it is more useful to focus on specific parameters that describe microtubule dynamic instability. These include microtubule growth rate, microtubule shortening rate, microtubule catastrophe frequency (switch from growing phase to shortening phase) and microtubule rescue frequency (switch from shortening phase to growing phase). As mentioned before, Tau interacts with microtubules with its microtubule binding domain, therefore, studies on Tau's regulation of microtubule dynamics have focused on the role of 3R and 4R isoforms of Tau (Weingarten et al., 1975; Witman et al., 1976; Drechsel et al., 1992; Esmaeli-Azad et al., 1994; Panda et al., 1995; Panda et al., 2003; Bunker et al., 2004; Levy et al., 2005; Bunker et al., 2006b; LeBoeuf et al., 2008b). In these studies, the analysis of results has focused on the number of microtubule binding repeats of Tau and the results have been generalized for all the isoforms containing those microtubule binding repeats.

Here we describe the results obtained from a meta-analysis of studies (Weingarten et al., 1975; Witman et al., 1976; Drechsel et al., 1992; Esmaeli-Azad et al., 1994; Panda et al., 1995; Panda et al., 2003; Bunker et al., 2004; Levy et al., 2005; Bunker et al., 2006b; LeBoeuf et al., 2008b) which focused on Tau's regulation of microtubule dynamics (Figure 6). According to the meta-analysis 4R isoforms largely affect the microtubule shortening rate and microtubule catastrophe frequency. More specifically, microtubule shortening rate and microtubule catastrophe frequency is decreased and therefore, 4R isoforms can be said to 'stabilize microtubules against shortening'. As far as microtubule growth rate is

concerned, the meta-analysis shows that there is no consensus regarding 4R isoforms effect on these parameters. 4R isoforms have been shown to, both, increase the microtubule growth rate and decrease the Microtubule growth rate.

According to the meta-analysis, 3R isoforms show no effect on microtubule rescue frequency. As far as the other parameters of dynamic instability are concerned, we find that there is no consensus regarding them. 3R isoforms have been shown to increase, decrease or not affect the microtubule growth rate at all. But it is important to note that this lack of consensus might be due to the finding that 3R isoforms regulate microtubule growth rate in a concentration dependent manner. At low Tau to tubulin ratio 3R isoforms decreases the microtubule growth rate and at high Tau to tubulin ratio 3R isoform increase the microtubule growth rate. This can be a reason for the lack of consensus regarding 3R isoforms regulation of microtubule growth rate. But as far as lack of consensus on 3R isoforms effect on microtubule shortening rate and microtubule catastrophe frequency is concerned, no reasonable explanation can be given. 3R isoforms have been shown to decrease or not affect the microtubule shortening rate. As far as microtubule catastrophe frequency is concerned, 3R isoforms have been shown to both, increase the microtubule catastrophe frequency and decrease the microtubule catastrophe frequency.

In summary, despite extensive study, Tau's regulation of different parameters of microtubule dynamic instability is still an open question (Weingarten et al., 1975; Witman et al., 1976; Drechsel et al., 1992; Esmaeli-Azad et al., 1994; Panda et al., 1995; Panda et al., 2003; Bunker et al., 2004; Levy et al., 2005; Bunker et al., 2006b; LeBoeuf et al., 2008b). More importantly the mechanism by which Tau regulates microtubule dynamics remains unknown.

	MT growth rate	MT shortening rate	MT catastrophe frequency	MT rescue frequency
4RL tau	↑[3] ↑[1] ↓[2]	↓[3] ↓[1] ↓[2]	↓[1] ↓[2]	↑[2]
4RS tau	↑[7] ↑[5] ↓[4] ↓[6]	↓[6] ↓[4]	↓[7] ↓[5]	
3RL tau	↑[3]	[3] NC		
3RS tau	↑[5] ↓[6] ↓[7] [4]NC	↓[6] [4]NC	↑[4] ↓[7] ↓[5]	[4]NC

1- Drechsel *et al,* 1992. 2- Panda *et al,* 1995. 3- Panda *et al,* 2003. 4- Bunker *et al,* 2004. 5- Levy *et al,* 2005. 6- Bunker *et al,* 2006. 7- LeBoeuf *et al,* 2008.

Figure 5: A meta-analysis of research studying Tau's regulation of microtubule dynamics.

1.4.3. Tau's interaction with microtubules

Understanding Tau's interaction with microtubules is critical to understanding its functions. Disruption of these interactions might also be involved in the early stages of tauopathies like Alzheimer's disease. Initial studies of Tau-Tubulin interactions focused on the Microtubule binding repeats of Tau as it is the primary site of interaction between Tau and Microtubules (Butner and Kirschner, 1991; Gustke et al., 1994; Mandelkow et al., 1995). These studies showed that Microtubule binding repeats bind Microtubules through a series of numerous weak electrostatic interactions (Butner and Kirschner, 1991; Gustke et al., 1994; Mandelkow et al., 1995) and the 13-14 amino acid long linker regions between

the Microtubule binding repeats do not directly interact with the Microtubules (Butner and Kirschner, 1991; Gustke et al., 1994; Mandelkow et al., 1995). Building on this model, later studies confirmed the delocalized interactions between Microtubule binding repeats and Microtubules, but regions of stronger discrete interactions were also found. More specifically, the linker region between Microtubule binding repeat 1 and Microtubule binding repeat 2 (IR1), binds microtubules with twice the binding affinity of any individual Microtubule binding repeat (Goode and Feinstein, 1994). Interaction between IR1 and Microtubules is also significant as IR1 is only present in 4R isoforms hinting to functional differences between the 3R and 4R isoforms (Goode et al., 2000).

Interaction between Tau and microtubules is also dependent on the region flanking the Microtubule binding repeats; proximally the proline rich region and distally the pseudo repeat region (Trinczek et al., 1995; Preuss et al., 1997; Mukrasch et al., 2007). In fact, peptides which have the Microtubule binding repeats and the flanking regions show highly enhanced binding to microtubules, compared to peptides which only have Microtubule binding repeats (Trinczek et al., 1995; Preuss et al., 1997; Mukrasch et al., 2007). Peptides with just the flanking regions also bind microtubules more strongly than peptides which have Microtubule binding repeats and no flanking regions. This contrasts with the model presented in the earlier studies which were mentioned in the previous paragraph. But, functional assays, mostly involving light scattering assays, to measure the microtubule assembling ability and microtubule polymerization ability of Tau reveal that although peptides with only the flanking regions bind microtubules strongly, these constructs are not functional. Functionality is rescued with constructs in which Microtubule binding repeats are present in addition to the flanking regions. Constructs with only the

Microtubule binding repeats show limited functionality (Trinczek et al., 1995; Preuss et al., 1997; Mukrasch et al., 2007).

These observations have led to the 'jaws model' of microtubule binding. In this model the flanking regions act as jaws which are mainly involved in binding of Tau to microtubules with the Microtubule binding repeats acting as the functional domain of the protein. The flanking regions and the Microtubule binding repeats together constitute the Microtubule binding domain of Tau. This model has also been tested, in vivo, in CHO cells (Preuss et al., 1997).

The crucial point to note from the preceding discussion and the conclusions presented by the studies mentioned, is that Tau binding to microtubules is relatively weak. The implication of this relatively weak binding is that Tau shows motion along the microtubules and this motion has multiple components. The importance of this multi-component motion will be discussed in the proceeding sections.

1.4.4. Tau's motion along the Microtubules has 2 components

As mentioned earlier, the interaction of Tau with microtubules is relatively weak. and, therefore Tau's behavior when bound to microtubules is dynamic. The dynamicity is exhibited in two ways: 1- Tau exists in a state of equilibrium between freely diffusing unbound state in solution and a bound state on the Microtubules (Samsonov et al., 2004). 2. Tau bound to Microtubules displays motion along the microtubule lattice and this motion has a static component and a dynamic component (Figure 5) (Mercken et al., 1995; Konzack et al., 2007; Hinrichs et al., 2012). In the dynamic component of motion, movement occurs in both directions of the microtubules and, evidence suggests that Tau can also switch protofilaments during the course of the dynamic component (Samsonov et

al., 2004). This multi component mode of motion of Tau on microtubules has physiological consequences as the state of equilibrium between the two components of motion modulate Tau's ability to regulate motor directed transport. Statically bound Tau can act as a barrier for molecular motors moving along the microtubule surface, but as Tau's motion also has a dynamic component, therefore, a Tau molecule cannot act as a permanent barrier for molecular motors.

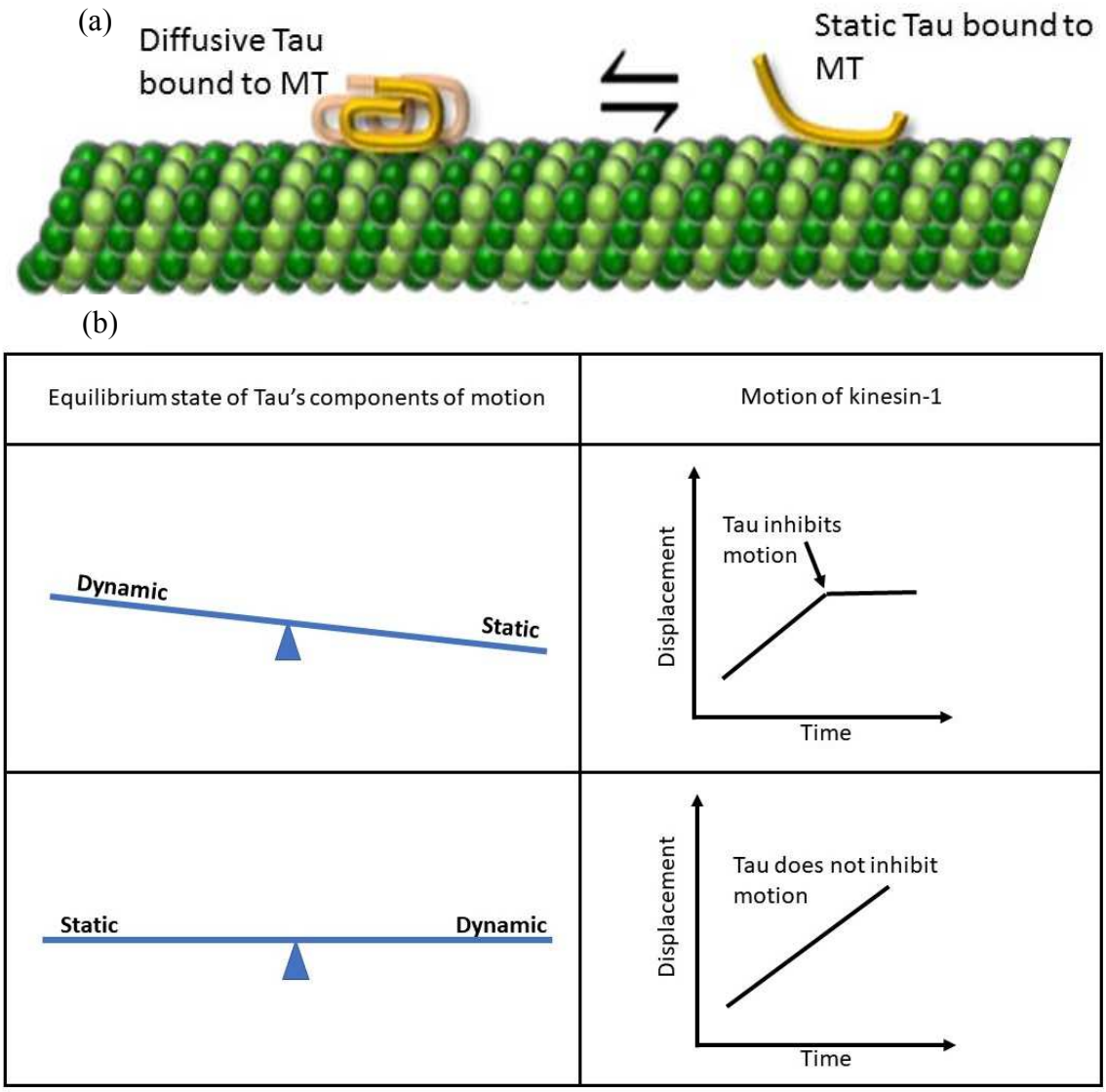

Figure 6: (a)Tau shows multiple components of motion when bound to the microtubule: Dynamic component and a static component. (b) Inhibition of kinesin-1 by Tau depends on the equilibrium between the dynamic and static components of Tau.

1.4.5. Tau's inhibition of molecular motors is dependent on the equilibrium between the 2 components of motion

Neurotransmitters, proteins and many other components required for axonal integrity, need to be transported to or from the cell body along the axon. One of the major functions of Tau includes regulation of axonal transport. *In vivo*, studies have shown that

disrupting Tau's activity alters the balance between anterograde (away from the cell body) and retrograde (towards the cell body) transport (Trinczek et al., 1999; Stamer et al., 2002; Mandelkow et al., 2003; Stoothoff et al., 2009b). In CHO cells transfected with Tau, anterograde transport is affected relatively more than retrograde transport, resulting in retraction of mitochondria towards the cell body. In a similar but different experiment Tau overexpression leads to a failure of transport of mitochondria to axons in CHO cells and differentiated neuroblastoma N2a cells. Similarly, in cultured neurons, Tau inhibits anterograde transport of peroxisomes, neurofilaments and Golgi-derived vesicles (Trinczek et al., 1999; Stamer et al., 2002; Mandelkow et al., 2003; Stoothoff et al., 2009b).

Single molecule experiments show that one way in which Tau regulates axonal transport is selective inhibition of molecular motors. This is dependent on a number of factors: 1- the isoform of Tau, 2- the molecular motor (Kinesin or Dynein) involved, and 3- the underlying microtubule lattice (Seitz et al., 2002; Vershinin et al., 2007; Dixit et al., 2008b; Vershinin et al., 2008; McVicker et al., 2011b; McVicker et al., 2014). Tau's inhibition of Kinesin, which carries cargo away from the cell body is more profound than its inhibition of Dynein, which transports cargo in the reverse direction. Kinesin is inhibited at one tenth of the concentration of Tau required to inhibit Dynein. Even concentrations of Tau that completely block Kinesin binding to microtubules, do not block Dynein binding (Dixit et al., 2008b). In summary, Tau has more of an impact on Kinesin dependent transport than it has on Dynein dependent transport

Apart from its dependence on the molecular motor involved, modulation of axonal transport by Tau is also isoform specific. 3RS isoform of Tau is more inhibitory to Kinesin-1 than the 4RL isoform. An important point to note is that 3RS isoform's motion along the

microtubule is biased towards the static component., whereas, for 4RL isoform the equilibrium between the static and dynamic components shows no bias towards either of the components (McVicker et al., 2011b; McVicker et al., 2014). Moreover, Phosphorylation of 3RS isoform at site Y18E alters the equilibrium of 3RS isoform motion and the bias towards the static component shown by 3RS isoform is removed (it behaves like the 4RL isoform). Consequently, like 4RL isoform its ability to inhibit Kinesin-1 is also reduced (Stern et al., 2017).

The discussion above shows that molecular motor inhibition by Tau and consequently, its ability to regulate axonal transport is dependent on the equilibrium between the two components of Tau's motion along microtubules (Figure 6b). Therefore, quantifying the multi component motion of Tau along the microtubule lattice is critical to understanding its function and its role in molecular motor inhibition. Development of a tool that performs this quantification in an automated, objective and time-efficient manner will be a major contribution towards the study of Tau.

1.5. Cargo transport towards axon terminal is carried out by a family of Kinesin motors

1.5.1. Structure of Kinesin motors

Kinesins act as cellular vehicles to transport material along the axon. For this they need to bind the cargo that needs to be transported. They also need to bind microtubules which serve as tracks for kinesin motion. There are two different regions of kinesin motors for cargo binding and Microtubule binding. Kinesin motors have a head domain which binds to the microtubules and shows motor activity. The head is linked to a filamentous

stalk which is linked to the globular tail. Cargo attachment occurs at the tail of a Kinesin motor (Hirokawa et al., 1989; Yang et al., 1989).

Based on the location of the head domain of kinesin motors, they are divided into 3 types: N-kinesins, M-kinesins and C-kinesins. N-kinesins have the head domain in the N-terminal region of the amino acid sequence, whereas, C-kinesins have the head domain in the C-terminal region of the amino acid sequence. In M-kinesins, the head domain is in the middle of the amino acid sequence (Aizawa et al., 1992). Classification based on the location of the head domain is important as this determines the direction in which a kinesin motor moves along a microtubule. N-kinesins, an example being Kinesin-1, move towards the plus end of the microtubules, whereas C-kinesins, an example being *Ncd* protein, move towards the minus end of the microtubule. M-kinesins move towards both directions (Aizawa et al., 1992). Apart from the classification mentioned above, kinesins are also grouped based on structural and functional differences. Based on this grouping 14 kinesins have been discovered (Dagenbach and Endow, 2004; Lawrence et al., 2004).

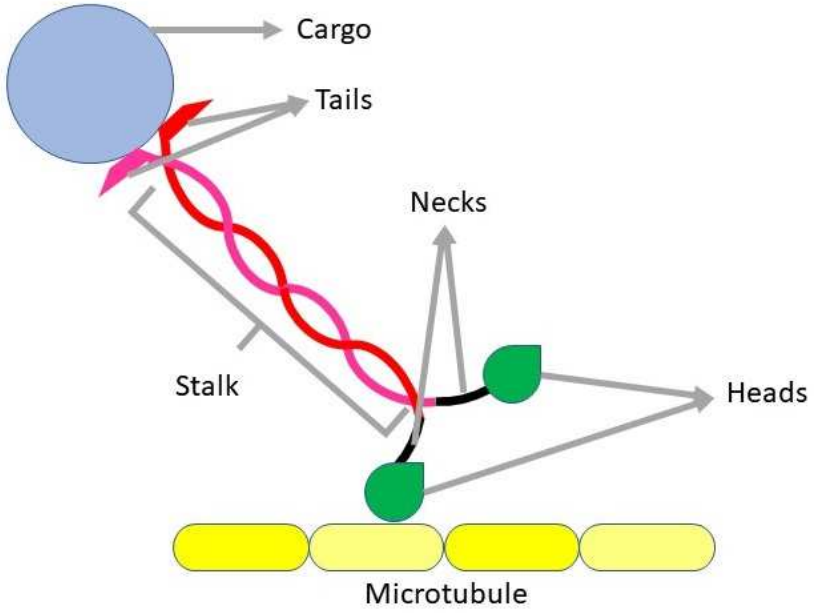

Figure 8: Structure of Kinesin dimer: Head domains bind to the microtubule, which are connected through a stalk to Kinesin tails, where the cargo binds.

1.5.2. Mechanism of Kinesin motor movement.

Kinesin motors move along the microtubule by converting chemical energy through hydrolysis of Adenosine-tri-phosphate (ATP) to mechanical energy. The head domain of kinesin motors possesses an ATP binding site. In the nucleotide free state, the Kinesin motor attaches to the microtubule (Okada and Hirokawa, 2000). Upon binding of ATP to the head domain of kinesin motor, there is a conformational change in the neck linker region (region that connects the head of a kinesin motor to the stalk) of kinesin motor which results in the rotational movement of the head domain (Rice et al., 1999). Upon ATP hydrolysis and subsequent phosphate release the head domain detaches from the microtubule. In a dimeric kinesin this cycle of ATP binding to phosphate release translates to the movement of one head domain while the other head domain is attached to the

microtubule. The repetition of this cycle results in movement in a step wise manner of kinesin motor along the microtubule lattice with a step size typically being 8 nm (Svoboda et al., 1993).

1.5.3. Biophysical properties associated with Kinesin motors

In vitro studies in which individual kinesin motors moving along the microtubules have been imaged, have been conducted to study the biophysical properties of these motors. Such properties include parameters such as motor velocity, motor run length (distance travelled by a motor without detaching from the microtubule lattice) and motor dwell time (time a motor spends on the microtubule lattice without detaching).

Kinesin-1 moves along the microtubule surface in a directed fashion making it relatively simple to obtain these parameters. But, introducing Tau in the system makes analysis of this data relatively complex, as kinesin-1 now pauses at locations where Tau is bound and detaches frequently (Dixit et al., 2008a; Stoothoff et al., 2009a; McVicker et al., 2011a; Stern et al., 2017). Consequently, single, directed component kinesin-1 motion, becomes multi component. Analysis of this motion needs to include the following additional components: kinesin-1 dwell time for the paused (or static) component, the frequency of pauses and the number of times kinesin-1 successfully navigates the Tau barrier. Analysis of kinesin-2 motion is similarly complex and the same parameters, as were needed for kinesin-1, need to be calculated. But the complexity of data analysis increases even more in the case of kinesin-3.

1.5.4. Role of Kinesin-3 in the context of the current study

For the current study, kinesin-3 is an ideal candidate as it displays 3 different components of motion. It has been shown that kinesin-3 can move along the microtubule lattice in a directed manner and it can also show non-directed movement on the microtubule lattice. Recently, kinesin-3 has been shown to switch between the 3 components of motion: directed, non-directed and static[1].

For this study, analyzing kinesin-3 SPT data is extremely enticing as it shows transitions between non-directed, directed and static components. For a complete biophysical characterization of kinesin-3, not only the transitions need to be identified and counted, but dwell times for different components of motion, alpha values (which differentiates between directed and non-directed motion), step size for non-directed component of motion and velocity for the directed component of motion needs to be measured. For these reasons, analysis of experimentally obtained kinesin-3 SPT data will be ideal to highlight the capabilities of the SPT data analysis tool. In the next chapter we discuss a novel analysis tool that is automated, user-friendly, less time-intensive and analyzes data in an objective manner. In the last section of the chapter we show the results obtained for kinesin-3 SPT data analyzed by the tool that we have developed.

[1] Unpublished data, courtesy of Dominique Lessard (Berger lab)

CHAPTER 2: ANALYSIS OF SINGLE PARTICLE TRACKING DATA FOR MULTI COMPONENT MOTION

2.1. The need for an automated, user-friendly, time-efficient tool

Chapter 1 highlights a few examples of biological phenomenon where SPT is being used to investigate functions of different proteins such as molecular motors and MAPs. Advances in microscopy such as Total Internal Reflection Microscopy (TIRF), which allows *in vitro* studies of cytoskeletal proteins with high signal to background ratio and super resolution microscopy, with nearly 7-10 fold greater resolution (in the range of 10s of nm) have greatly facilitated the utility of SPT in studying motion of small intracellular structures, and even individual molecules (Thompson and Lagerholm, 1997; Pierce and Vale, 1999; Gustafsson, 2000; Schmoranzer et al., 2000; Toomre and Manstein, 2001; Betzig et al., 2006; Willig et al., 2006b; Willig et al., 2006a; Kellner et al., 2007; Willig et al., 2007; Schermelleh et al., 2008). We have focused on the use of SPT to study axonal transport, but another area where SPT is being extensively used is in the study of membrane properties (Pralle et al., 2000; Schutz et al., 2000; Eggeling et al., 2009; Sahl et al., 2010; Vicidomini et al., 2015; Abboud et al., 2018). Moreover, numerous techniques and methods have been developed which allow users to track single molecules in images obtained from microscopy with high accuracy and, in some cases, in an automated manner (Sage et al., 2005; Jaqaman et al., 2008; Ram et al., 2008; Ruhnow et al., 2011; Liu et al., 2013; Chaphalkar et al., 2016; Mangeol et al., 2016; Xiao et al., 2016). But few tools exist for analyzing the SPT data in an automated, user-friendly, time-efficient and objective manner. Therefore, there is a critical need for the development of such a tool.

To address this need we have developed a MATLAB program called Mixed Motion Analysis (MixMAs), which takes SPT data as input and analyzes it using a sliding window analysis technique. The users only need the SPT data, an estimate of the error in determining the position of the tracked particle and an estimate of the size of the step, in the time interval between 2 consecutive image frames, of their particle of interest. MixMAs then analyzes the SPT data and outputs the parameters required for complete characterization of the multi component motion of the particle. In the following sections the techniques used to develop MixMAs, the validation of MixMAs using simulated data and application of MixMAs on Kinesin-3 SPT data is presented.

2.2. Methods

2.2.1. Data needed to use MixMAs

The data used as input to MixMAs is the tracking data generated from imaging fluorescently labelled single molecules and tracking them (i.e., getting their position (X-coordinate, Y-coordinate)). These coordinates need to be stored in an excel file with different columns for identification labels of different particles, X-coordinates of different particles and Y-coordinates of different particles. The columns do not need to have any specific order as the program asks the users to input the excel column label where identification labels of particles, their X-coordinates and their Y-coordinates are stored. This excel file is referred to as the coordinates file. This coordinates file is an input to MixMAs which it uses to analyze particle's motion.

Apart from the coordinates file, an estimate of the error in determining the position of the tracked particle is also needed. This error is referred to as the localization error. The localization error depends on the resolving power of the microscope and the accuracy of

the tracking method used. An estimate of the size of the step, in the time interval between 2 consecutive image frames, of their particle of interest, in μm is also needed. This is referred to as the step size.

2.2.2. Algorithm

The algorithm uses the following steps for analyzing motion of particles:

1- Coordinates file is read and events which appear for a number of image frames that is lower than a user supplied minimum value are removed. Coordinates for every particle are stored in individual cells (A MATLAB data type).

2- For every particle the displacement for each time step and the smallest angle, that two such displacements make, from the positive X-axis is calculated Both these values are stored in different vectors (A MATLAB data type).

3- Sliding window analysis is performed on the displacement vector generated in step 2, and regions within the window are classified into dynamic or static components using a cutoff value

4- Sliding window analysis is performed on the angle vector, generated in step 2, for the dynamic components identified in step 3, and the regions are further sub-classified as directed or non-directed using another cutoff value. Non-directed, static and directed components are given identification values of 1,2 and 3 respectively. These values are stored in a vector (A MATLAB data type).

5- The cutoff values, mentioned in step 3 and 4, are generated by simulating motion of particles using 2 estimates that the user provides. The first of these is the step size of the particle and the second estimate is the localization error.

6- Using the identification values vector, generated in step 4, transitions between different states are identified and dwell times for different states, transition frequencies for different transitions, alpha values for different components, step size (for non-directed motion), and velocity (for directed motion) are calculated. These parameters stored in a structure (A MATLAB data type). This is the output that is generated by MixMAs.

2.2.3. Displacement and angle calculation

X and Y coordinates are used to calculate displacement between two points. For particle k the displacement s^k_i between time points i and $i+1$ is calculated:

$$s_i^k = \sqrt{(x_i^k - x_{i+1}^k)^2 + (y_i^k - y_{i+1}^k)^2}$$

The displacement values for particle k are stored in a vector:

$$S^k = [s_i^k, s_{i+1}^k, \ldots..]$$

X and Y coordinates are also used to calculate the smallest angle that a displacement vector s_i^k makes with the positive X-axis:

$$\theta_i^k = abs\left[\tan^{-1}\left(\frac{(y_{i+1}^k - y_i^k)}{(x_{i+1}^k - x_i^k)}\right)\right]$$

To ensure that θ_i^k is calculated from the positive X-axis the following checks are implemented in the program:

- if $\left(y_{i+1}^k - y_i^k\right)$ is > 0 and $\left(x_{i+1}^k - x_i^k\right)$ is < 0, θ_i^k is subtracted from 180 and the result is used as θ_i^k.
- if $\left(y_{i+1}^k - y_i^k\right)$ is < 0 and $\left(x_{i+1}^k - x_i^k\right)$ is < 0, θ_i^k is added to 180 and the result is used as θ_i^k.
- if $\left(y_{i+1}^k - y_i^k\right)$ is < 0 and $\left(x_{i+1}^k - x_i^k\right)$ is > 0, θ_i^k is subtracted from 360 and the result is used as θ_i^k.

To ensure that the smallest value of θ_i^k from the positive X-axis is calculated the following check is implemented in the program:

- If θ_i^k is > 180, θ_i^k is subtracted from 360 and the result is used as θ_i^k.

The angle values for particle *k* are stored in a vector:

$$\dot{\theta}^k = [\theta_i^k, \theta_{i+1}^k, \ldots..]$$

2.2.4 Sliding window analysis to identify transition points

Sliding window analysis is performed on the generated vector $\dot{\theta}^k$ and S^k, and two parameters are calculated for each step *i* of the window: 1- $Movement_i^k$: the maximum of the displacements within the window and 2- $Direction_i^k$: the standard deviation of angles within the window (Figure 8). If the movement parameter is greater than a user specified cutoff value then the component of particle's motion within the sliding window is classified as dynamic, otherwise it is classified as static. For dynamic component, if the direction parameter is greater than a user specified value then the component is further sub classified as non-directed, otherwise it is sub-classified as directed. In this way, a component vector for particle *k* is generated for every step of the window. Within the vector, 1 designates non-directed, 2 designates static and 3 designates directed motion:

$$Component^k = [2, 2, 2, 3, 3, 1, \ldots]$$

The component vector is then refined by combining consecutive similar components. The component vector is then checked for changes of components. The frame where a component change occurs, is classified as a transition and a transition vector, containing the frame number, for particle k is generated:

$$Transition^k = [5, 10, 22, \ldots]$$

The transition vector is refined by adding a start value of the trajectory, frame at which a trajectory started, and the end value of the trajectory, frame at which the trajectory ended. The default length of the sliding window is two time intervals but the users have the option to change this value. All the analysis performed in this study use the default value of the sliding window size.

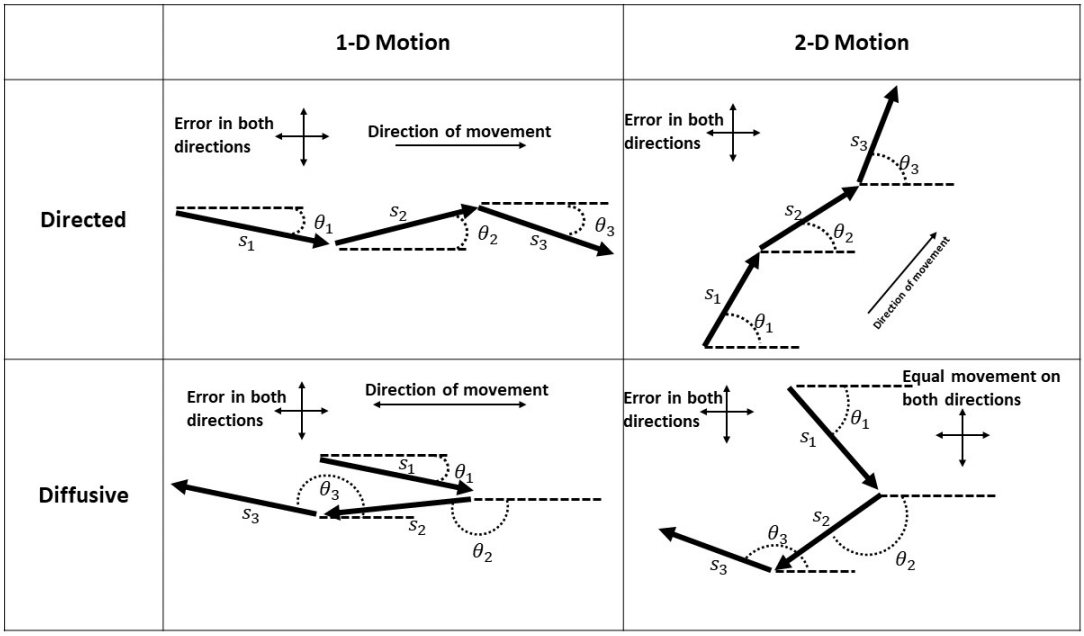

Figure 9: Calculation of two parameters for a sliding window of size 3: Four example trajectories with three steps each are shown. For every step a displacement value (s) and the smallest angle (θ) from the positive X-axis is calculated. Parameter 1 is the maximum of the three displacements (s_1, s_2, s_3) and parameter 2 is standard deviation of the three angles (θ_1, θ_2, θ_3). If parameter 1 is greater than a specified movement cutoff value then the region is classified as dynamic. If, for a dynamic region, parameter 2 is greater than a specified direction cutoff value then the region is sub classified as diffusive.

2.2.5. Calculation of movement and direction cutoff values

Simulation of static particles, diffusive particles and directed particles is performed which uses a user specified input value of the estimated step size of the particle and an estimated value of the localization error for the particle in μm (Figure 12).

To calculate the Direction cutoff value, the script called FindDiffusiveDirectedCutoff for 2-dimensional (2-D) motion analysis and FindDiffusiveDirectedCutoff1D for 1-dimensional (1-D) motion analysis is run. Both the scripts are identical with the exceptions that in the 1-D script, motion occurs only in the horizontal direction and variations in vertical direction are due to the localization error.

Using FindDiffusiveDirectedCutoff script, 200 diffusive particles and 200 directed particles are simulated. Sliding window analysis is then performed and the direction parameter is calculated and stored (Figure 8). A range of direction cutoff values are then tested and regions where the direction parameter is greater than the direction cutoff value is classified as diffusive, otherwise it is classified as directed. For every direction cutoff value tested the percentage of diffusive components that are missed (% diffusive missed) and the percentage of directed components that are missed (% directed missed) is calculated (Figure 9a). The direction cutoff value at which both the missed events, % diffusive missed (Figure 9d) and % directed missed (Figure 9c) are minimized is stored. The entire process is repeated 100 times and the mean of the direction cutoff values is calculated. This is the suggested direction cutoff value that a user should use for performing analysis with MixMAs (Figure 9b).

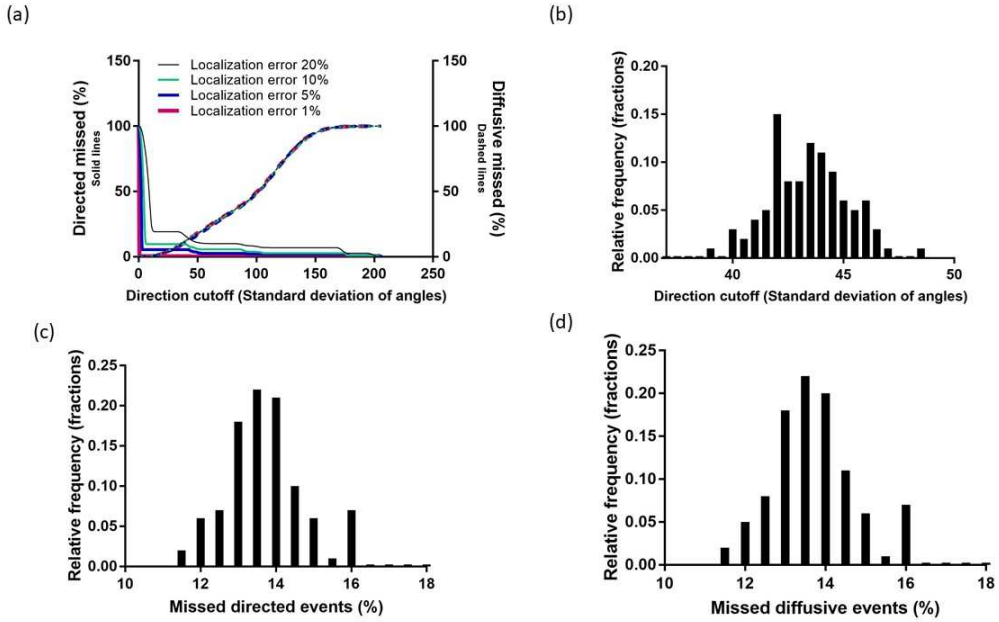

Figure 10: (a) Plot of direction cutoff value (used for separating diffusive and static components) and the % of missed events for different values of localization error. The value where the diffusive missed (%) is equal to the directed missed (%) is recorded. The simulation is run 100 times to generate (b) 100 direction cutoff values, (c) 100 missed directed component (%) values and (d) 100 missed diffusive component (%) values. Mean of (b) the direction cutoff values is suggested to be used in MixMAs.

.

A similar process is used for calculating the movement cutoff value, except for the following changes:

- Static and diffusive or diffusive and directed particles are simulated instead of diffusive and directed particles. The default that the script uses is static and diffusive particles.
- Movement parameter is used instead of direction parameter.
- FindDynamicStaticCutoff script is used instead of FindDiffusiveDirectedCutoff for 2-D analysis and FindDynamicStaticCutoff1D script is used instead of FindDiffusiveDirectedCutoff for 1-D analysis.

2.2.6. Simulation of particles to generate coordinates files

200 particles are simulated to generate coordinates files which are then analyzed by MixMAs. Simulations are performed both in 1-D, using the script Mixed Motion Simulation 1-D (MixMSi1D), and in 2-D, using the script Mixed Motion Simulation (MixMSi). To simulate the motion of a particle it is given a starting *x* and *y* position of 10 μm. Then, after every iteration these positions are changed based on the component of the motion. The particle's position is updated 10 times for each component of motion. The order of components used in the simulations are as follows:

[Directed, Static, Diffusive, Directed, Diffusive, Static, Directed]

As there are a total of 7 components with each being updated 10 times simulation of a single particle generates a total of 70 positions. In an experimental setup this will translate to 70 frames. For 2-D directed motion the positions are updated in the following way:

$$x_t = x_{t-1} + \{DirectedStepSize \times \cos(RandomAngle[0-360])\} + \{LocalizationError \times \cos(RandomAngle[0-360])\}$$

$$y_t = y_{t-1} + \{DirectedStepSize \times \sin(RandomAngle[0-360])\} + \{LocalizationError \times \sin(RandomAngle[0-360])\}$$

In the above equations for a continuous directed motion the RandomAngle is chosen only once, at the start of the directed motion, and then the same angle is used until the end of the directed motion. For 2-D diffusive motion the same equations are used except that the RandomAngle is chosen whenever the position of a particle is updated and DiffusiveStepSize is used instead of DirectedStepSize. For static component, only the LocalizationError is added to update the particle position. For example, to update static *x* position "$\{LocalizationError \times \cos(RandomAngle[0-360])\}$)" is added to the previous

x position and to update y position "$\{LocalizationError \times \sin(RandomAngle[0-360])\}$" is added to the previous y position. In the static case, just as in the diffusive case, the RandomAngle is chosen whenever the position of a particle is updated.

Simulations for the 1-D particle motion utilize similar equations with a few changes which are outlined below:

- Only the x position is updated for all the components, while update of y position only involves adding the localization error multiplied with "$(RandomNumber[1\ or\ -1])$". The changes described below are only applied to the x position of the particles.
- For directed motion the DirectedStepSize is multiplied with "$(RandomNumber[1\ or\ -1])$" and the LocalizationError is also multiplied with "$(RandomNumber[1\ or\ -1])$". Like the 2-D case, the RandomNumber is chosen only once (at the start of the directed motion) and then the same angle is used until the end of the directed motion.
- For diffusive motion the DiffusiveStepSize is multiplied with "$(RandomNumber[1\ or\ -1])$" and the LocalizationError is also multiplied with "$(RandomNumber[1\ or\ -1])$". Like the 2-D case, the RandomNumber is chosen every time the particle's position is updated.
- For static component, only the LocalizationError is multiplied with "$(RandomNumber[1\ or\ -1])$". The RandomNumber is chosen whenever the position of a particle is updated.

Users can set a time interval value for an update in the position of a particle. The default value is set to 0.1s and this value is used in this study except otherwise stated. The resulting, coordinates values are stored in an excel file for further use in MixMAs.

2.2.7. Procedure to use the program

The procedure to use the program is shown in figure 10. Users are required to provide an estimate of the localization error in μm and the step size of the particle in μm. The program uses these two values to determine two cutoff values: 1- direction cutoff value, and 2- movement cutoff value. The two cutoff values along with the coordinates file are used as input to analyze the motion of particles.

The following scripts are used as part of the work flow:

- FindDynamicStaticCutoff: Finds movement cutoff value for 2-D analysis.
- FindDynamicStaticCutoff1D: Finds movement cutoff value for 1-D analysis.
- FindDiffusiveDirectedCutoff.: Finds direction cutoff value for 2-D analysis.
- FindDiffusiveDirectedCutoff1D: Finds direction cutoff value for 1-D analysis.
- MixMAs: The main program which takes as input the coordinates file and the cutoff values to analyze SPT data.

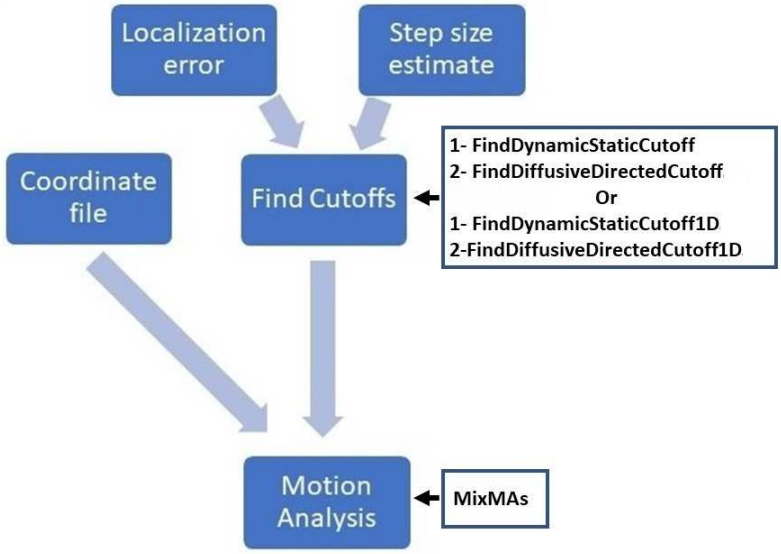

Figure 11: Workflow for motion analysis: An estimate of the step size of the particle and the error in the localization of the particles is used to simulate diffusive, static and dynamic events and two cutoff values (1- for separating dynamic and static events (Movement cutoff) and 2- for separating dynamic events into diffusive and directed events (Direction cutoff)) are generated using scripts indicated in the figure. These values and the coordinates file are then used as inputs for the motion analysis program, Mixed Motion Analysis (MixMAs).

2.2.8 Calculation of step size and alpha values

The first time that MixMAs is used it analyzes the motion of particles and outputs the results. It also calculates the mean squared displacement for each component of motion and saves it. The user can then run MixMAs again and choose the option of analyzing mean squared displacement which results in the output of an alpha value and the step size.

For every component of motion identified by MixMAs, the mean squared displacement and time interval for which this displacement was measured, is fit to the diffusion equation:

$$\langle X \rangle = aDt^{\alpha}$$

Where, $\langle X \rangle$ is the mean squared displacement, t is the time interval, D is the diffusion coefficient, a is the dimensionality factor, 2 for 1-D motion and 4 for 2-D motion, and α defines the component itself. In an ideal case, for diffusive component α is 1 and for directed component it is 2. A value of α less than 1 designated anomalous diffusion. The value of α obtained for our simulations and experimental data also ensure that MixMAs accurately separates the different components of motion.

To calculate mean squared displacement, it is first calculated for individual particles. Then the mean squared displacement of individual particles is averaged. To do this mean squared displacement for a specific time interval is averaged over all the particles to get a mean value and a standard deviation value for that time interval. As not all trajectories belonging to a specific component of motion are of the same length of time, $\langle X \rangle$ is fit up to the time interval for the particle which had the shortest trajectory. This ensures that there are equal number of particles that were averaged, for every value of $\langle X \rangle$.

We calculated the step size of a particle instead of directly using the diffusion coefficient since step sizes were used as input for the simulations performed. This made the comparison between the input given to the simulation and the result given by MixMAs easier.

2.3. Results

2.3.1 Validation using simulation of particles

We validated the algorithm by simulating motion of particles (Figure 11) using MixMSi script for 2-D simulations and MixMSi1D script for 1-D simulations. In both the scripts, 200 particles were simulated with the following input component vector:

[Directed, Static, Diffusive, Directed, Diffusive, Static, Directed]

Simulated motion produced an excel track file which was then used as an input with an estimate of step size and localization error to the analysis program, MixMAs (Figure 12). Simulations were performed for different values of the ratio of step size to localization error to check the robustness of MixMAs. The step size was fixed at 1 μm. Ratios of step size to localization error used in the simulations were 1%, 5%, 10%, 20% and 50%. Simulations were performed in 1-D and in 2-D. Every coordinate file generated from a simulation was analyzed using MixMAs and the results were saved. This was repeated 10 times, therefore, 10 values of the number of transitions, dwell times, alpha (α) values and step sizes were calculated. Then the mean and the standard deviation of these values was plotted alongside the input values used in the simulations.

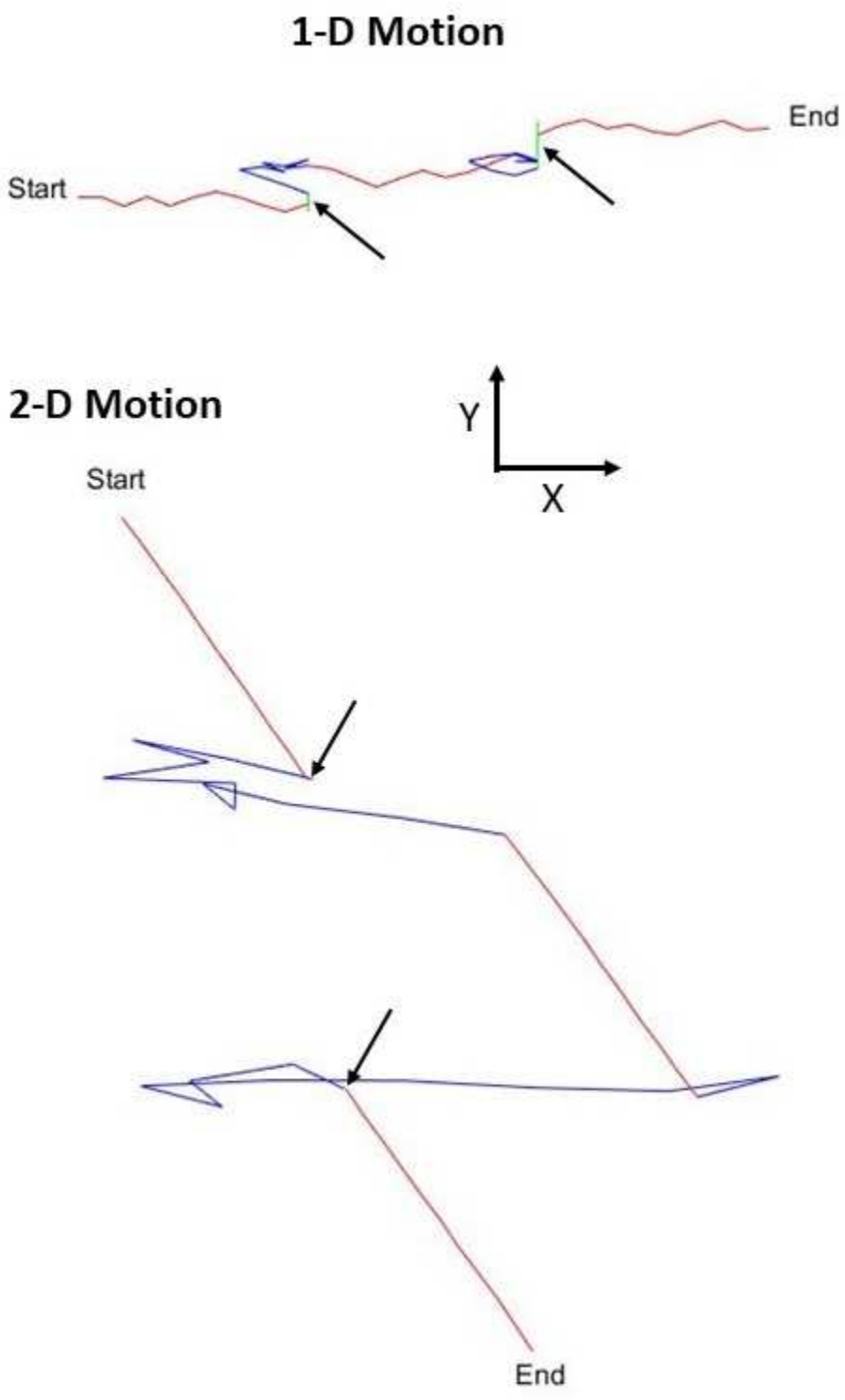

Figure 12: Motion Simulation: Motion in space of 2 simulated particles is shown. Every particle trajectory has 1 of each of the following: Directed (red) to static (green) transition, directed (red) to diffusive (blue) transition, static (green) to directed (red), static (green), to diffusive (blue), diffusive (blue) to static (green)

and diffusive (blue) to directed (red). As static motion in space is relatively small, arrows are used to highlight static regions.

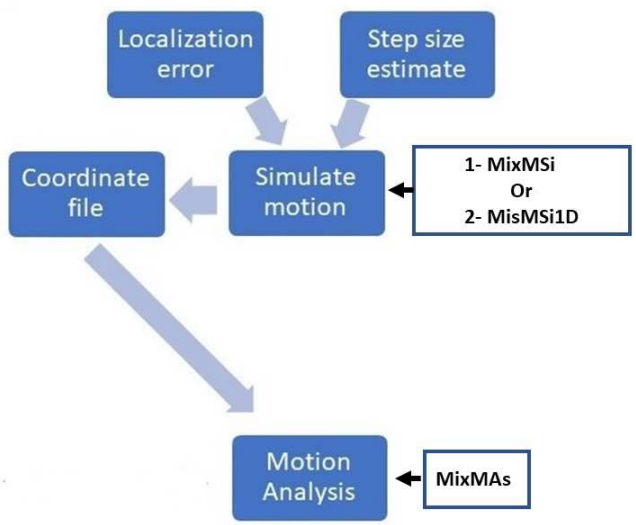

Figure 13: Motion is simulated by supplying localization error and step size estimates to scripts mentioned in the figure which then generate an excel coordinate file. This file can then be used as input for MixMAs.

The analysis results show that the algorithm is validated for a range of localization error values for both, 1-D and 2-D case (Figure 13, Figure 14, Figure 15, Figure 16). The number of transitions (Figure 13a) and dwell times calculated by the program (Figure 13b) are comparable to the input values given in the 1-D simulations. alpha values for diffusive component of motion are very close to 1 whereas the alpha values for the directed component of motion are very close to 2. This is true for all values of step size to localization error ratio that were tested (Figure 14a). Step sizes are calculated using alpha

values fixed (Alpha fixed) at 1 for diffusive component and 2 for directed component (Figure 14b). Similarly, step sizes are calculated using alpha values calculated in figure 14a (Alpha floating). Floating and fixed values of alpha generate similar results (Figure 14b).

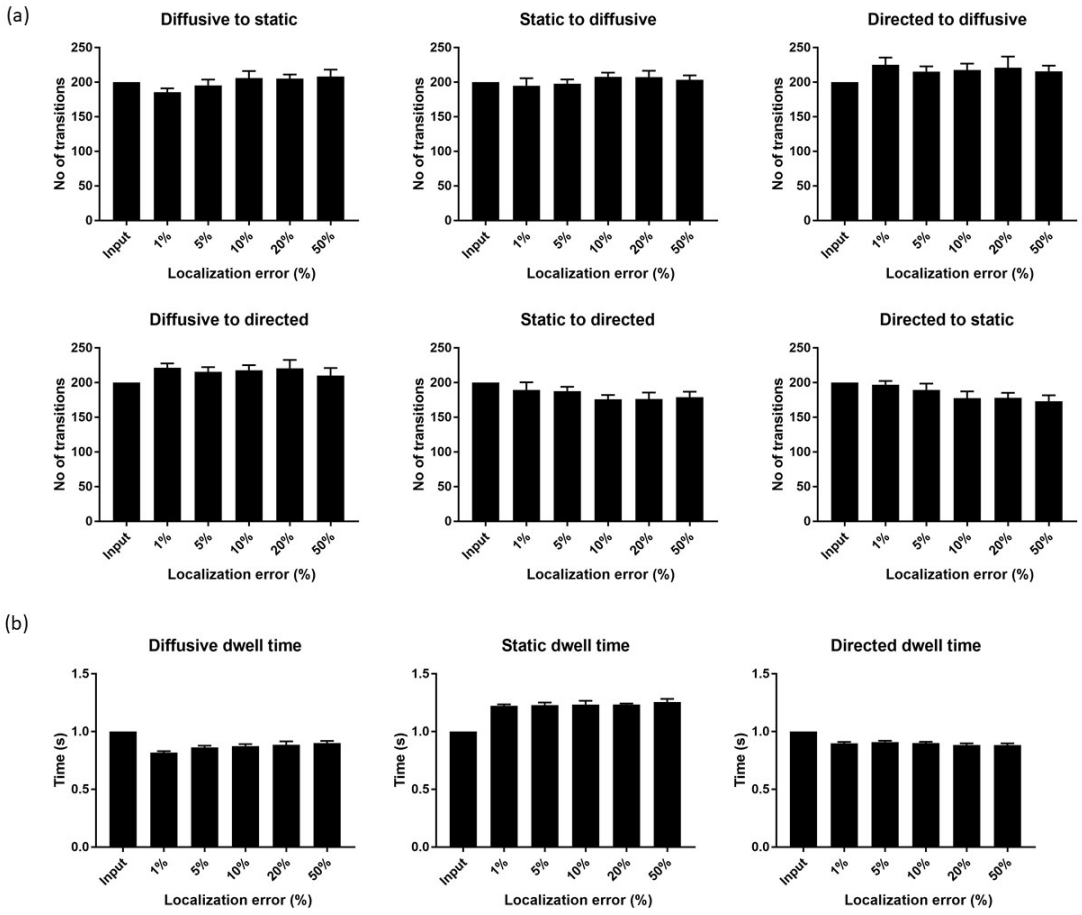

Figure 14: Results from motion of particles simulated in 1-D. 200 particles are simulated '(see figure 4 & 5)' for different values of localization error. For each localization error (%) the simulation is run 10 times. The number of different transitions is then calculated. (a) Plots for the mean number of transitions for different values of localization error are shown. (b) Plots of mean of the dwell times for different values of localization error are shown. The title of each graph shows the type of motion for which the dwell times are calculated, and for the type of transition that is observed. (Bars indicate standard deviation).

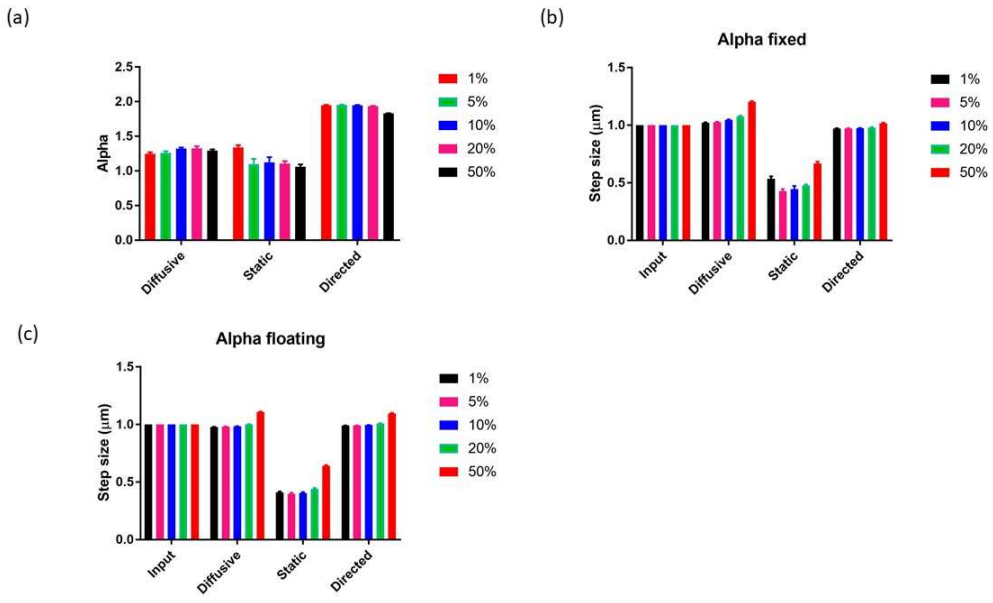

Figure 15: (a) Alpha values for diffusive, static and directed motion for different values of localization error are calculated for motion simulated in 1-D. Step size values for diffusive, static and directed motion for different values of localization error are calculated (b) using alpha value fixed at 1 for diffusive and static motion, and 2 for directed motion and (b) using alpha values calculated in (a). (Bars indicate standard deviation).

The algorithm was also validated for motion in the 2-D case as shown in figure 15 and figure 16. The results show that the program performs as well in the 2-D case as it does in the 1-D case.

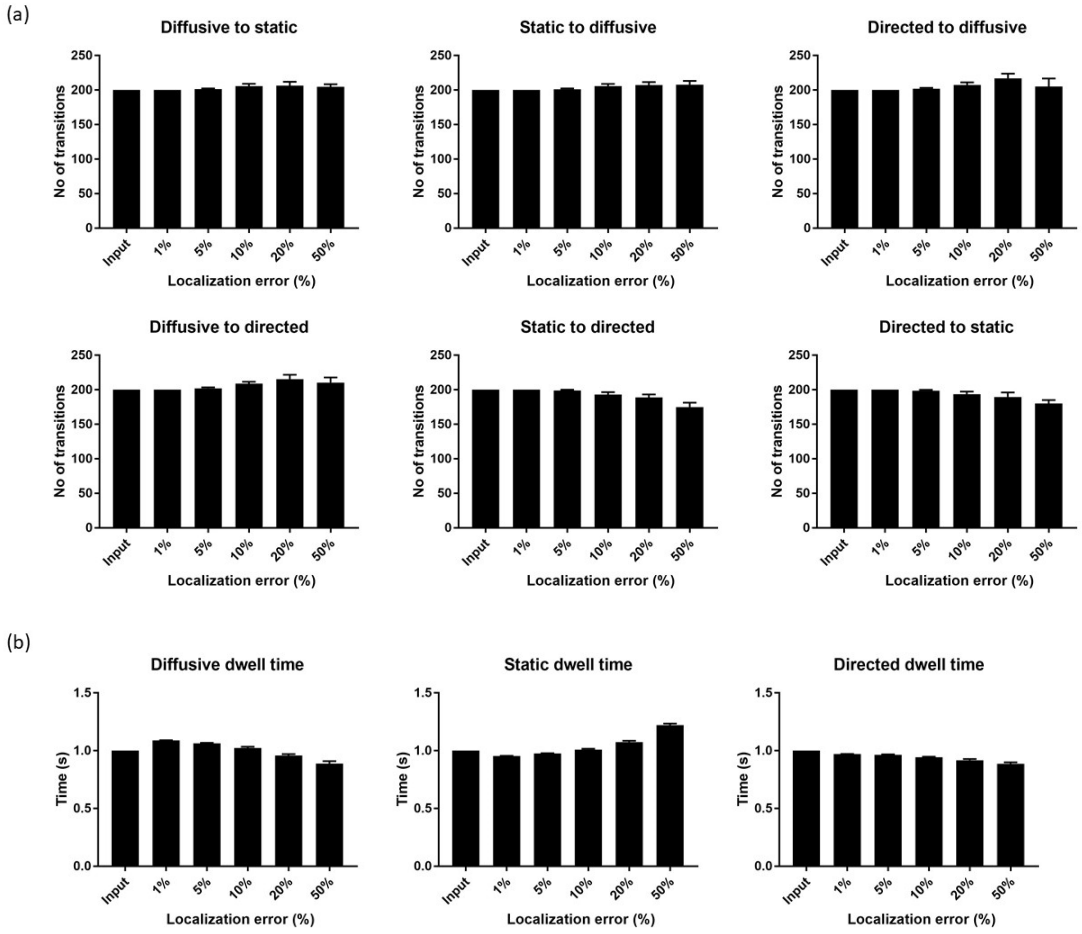

Figure 16: Results from motion of particles simulated in 2-D. 200 particles are simulated (see figure 4 & 5) for different values of localization error. For each localization error (%) the simulation is run 10 times. The number of different transitions is then calculated. (a) Plots for the mean number of transitions for different values of localization error are shown. (b) Plots of mean of the dwell times for different values of localization error are shown. The title of each graph shows the type of motion for which the dwell times are calculated, and the type of transition that is observed. (Bars indicate standard deviation).

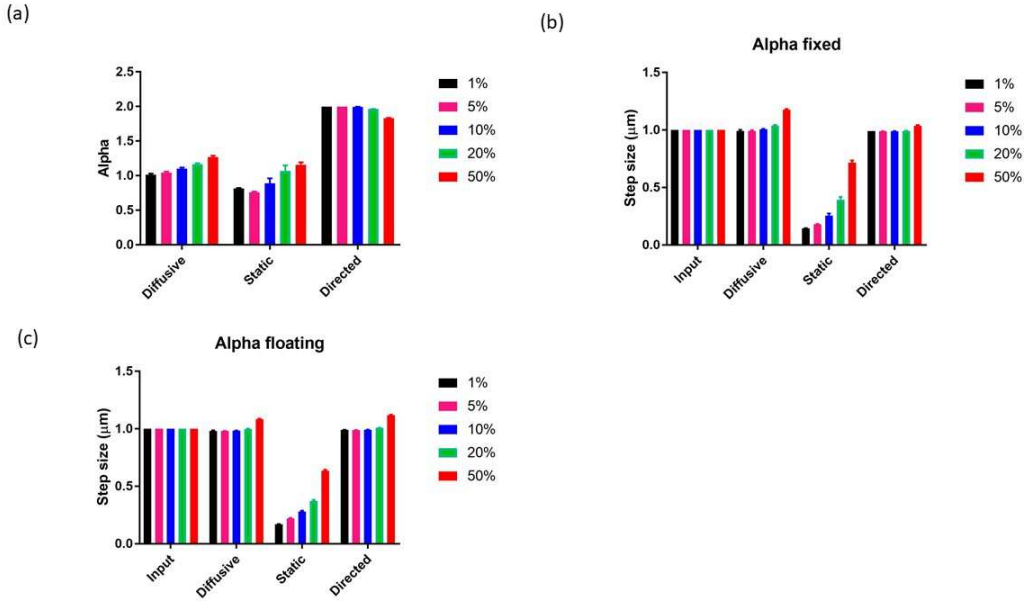

Figure 17: (a) Alpha values for diffusive, static and directed motion for different values of localization error are calculated for motion simulated in 2-D. Step size values for diffusive, static and directed motion for different values of localization error are calculated (b) using alpha value fixed at 1 for diffusive and static motion, and 2 for directed motion and (b) using alpha values calculated in (a). (Bars indicate standard deviation).

2.3.2. Application

Kinesin-3 shows 3 components of motion; diffusive, directed and static. These components transition between each other within a single run making experimentally collected kinesin-3 SPT data an ideal candidate for analyses using MixMAs.

To analyze kinesin-3 SPT data[2] the workflow shown in figure 3 was followed. Firstly, cutoff values were calculated by using an estimated step size of 0.2 µm and an estimated localization error of 0.2 µm. The cutoff scripts used were those for 1-D motion.

[2] Unpublished data, courtesy of Dominique Lessard (Berger lab)

These scripts yielded a movement cutoff value of 0.22 and direction cutoff value of 60º. These cutoff values along with an excel file containing coordinates data for 134 kinesin-3 molecules were input in MixMAs for analysis of kinesin-3 motion. The results obtained are shown in figure 18. The most important point to note in the figure is that for diffusive component of motion the alpha value is very close to 1 and for the directed component of motion it is very close to 2 (Figure 18d, 18f). This information is crucial as it increases confidence in the results obtained for the number of transitions, dwell times and velocity for Kinesin-3. To further validate these results, motion of kinesin-3 was simulated using MixMSi1D script with a step size of 0.4 μm and a localization error of 0.2 μm and a time interval value of 0.2s. The results of the simulation show that the input values for all the parameters are comparable to the values resulting from MixMAs analysis (Figure 19). This result combined with the alpha values obtained (Figure 18d, 18f) validates the results obtained for kinesin-3 with a high degree of confidence.

Looking at the fit between the mean squared displacements and time for diffusive and static components, we thought that the slopes of the fit (diffusion coefficients) for diffusive and static components are very close to each other. This raises a problem because, if true, this means that there is no difference between the static and diffusive components.

To explore this further we calculated diffusion coefficients for static and diffusive components for alpha values fixed at 1 and for alpha values shown in figure 18d and 18e (Figure 18g). The results show that using alpha values shown in figure 18d and 18e, there is no difference between the diffusion coefficients of the two components. But, this is not an ideal comparison as the alpha values for the two components are different. As, the alpha values for both the components are close to 1, it is reasonable to calculate the diffusion

coefficients for these two components using an alpha value fixed at 1. As shown in figure 18g when the alpha value is fixed at 1, there is indeed a difference between then diffusion coefficients of the static and diffusive components.

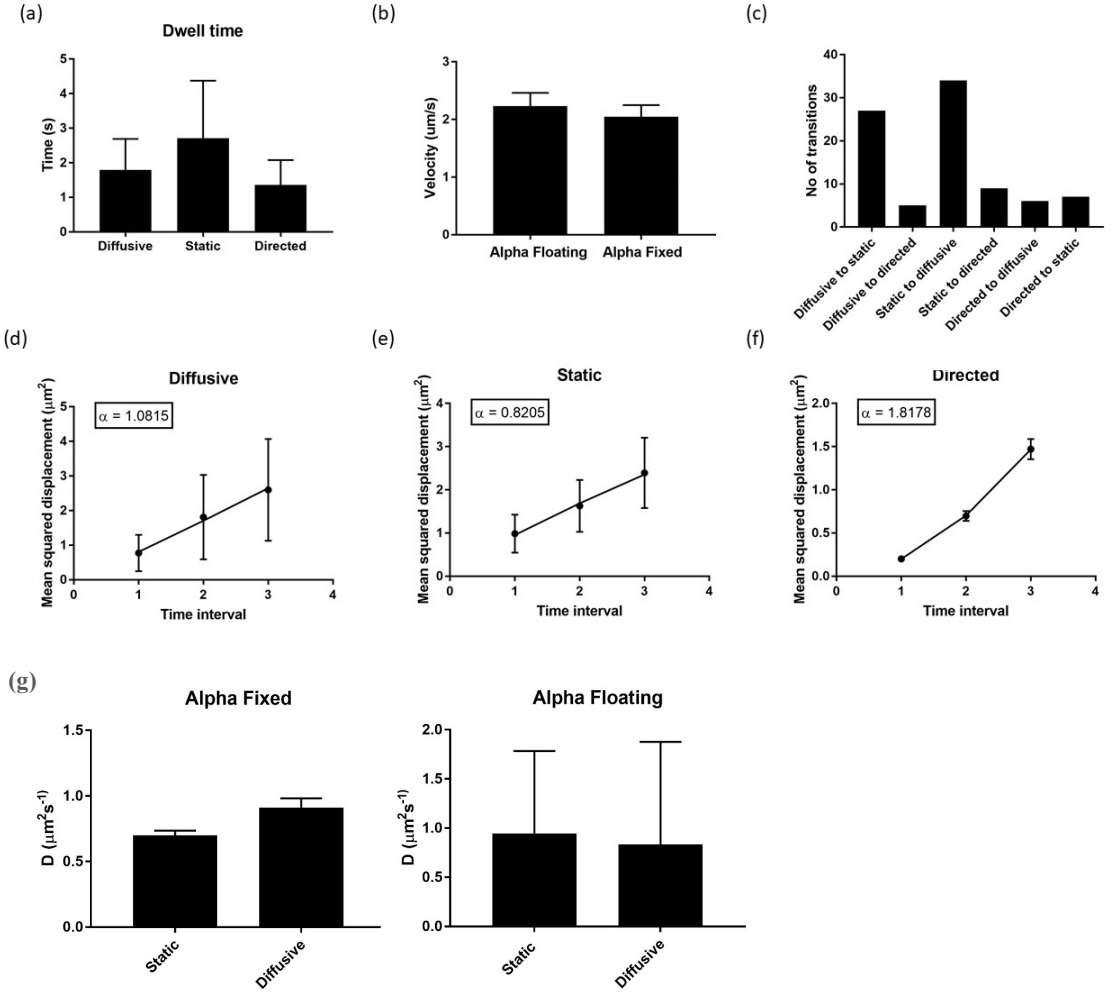

Figure 18: Motion of Kinesin-3 is analyzed and (a) dwell times for different states and (c) number of transitions are calculated. Alpha values for (d) diffusive, (e) static and (f) directed motion are also calculated. (b) Velocity for directed motion is calculated using alpha values (alpha floating) calculated in (f) and using a fixed alpha value of 2. Diffusion coefficients for static and diffusive components are shown

for alpha values fixed at 1 (alpha fixed) and for alpha values calculated in (f) (alpha floating). (Bars indicate standard deviation).

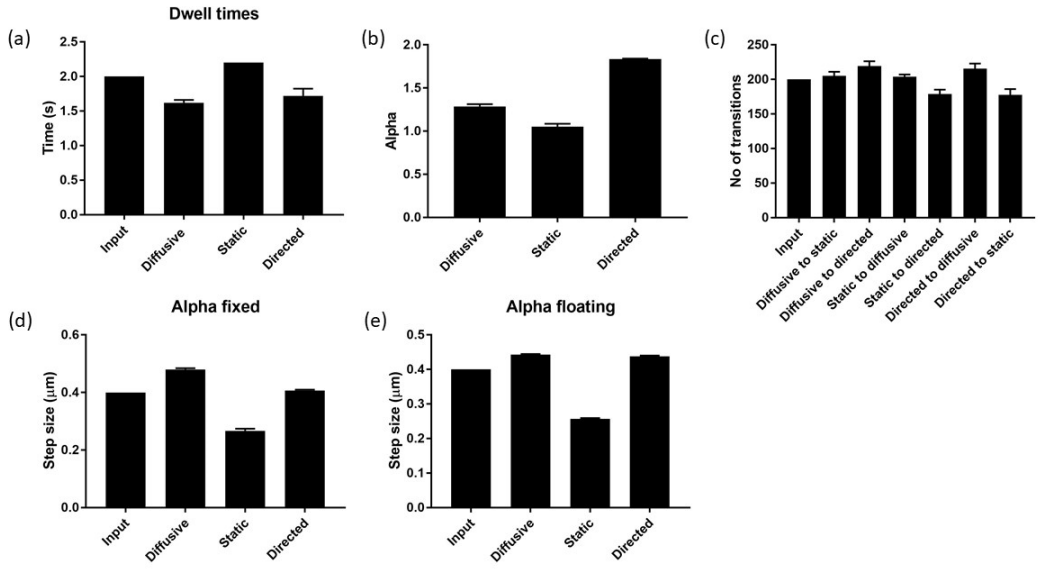

Figure 19: Kinesin-3 motion is simulated by simulating particle motion in 1-D with a step size of 0.4 μm for diffusive and directed motion with localization error of 0.2 μm. A total of 200 particles are simulated. The simulation is run for 10 times. (a) Mean dwell times for different states, (b) alpha values and (c) number of transitions are shown. Step size is calculated using (d) alpha value fixed at 1 for diffusive and static motion, and 2 for directed motion and (e) using alpha values calculated in (Alpha floating) (b). (Bars indicate standard deviation).

CHAPTER 3: DISCUSSION

3.1. Conclusions

We have developed a MATLAB program, called MixMAs, to analyze SPT data. To validate the analysis routine, we simulated motion of particles with multiple components of motion, both in 1-D and 2-D, and analyzed the simulated SPT data with MixMAs. The results of the validation show that MixMAs works accurately for a range of step size to localization error ratios. This is true for both 1-D and 2-D cases. Finally, experimentally obtained Kinesin-3 SPT data was analyzed with MixMAs and the results obtained show that MixMAs works accurately for experimentally obtained data as well. In summary, the MixMAs program analyzes SPT data for particles with multiple components of motion in an objective, automated, user friendly and time-efficient manner.

3.2. Features of the current implementation

3.2.1. Bias towards the dynamic component for motion length smaller than the size of the sliding window

Inherent to the sliding window analysis method used in the MixMAs program is a bias towards the dynamic component of motion when static events are smaller than the size of the sliding window. The reason for this is the use of the criteria of using maximum displacement, within a sliding window to classify dynamic and static components. The following 2 examples characterize the features of this limitation in detail.

Example 1:

Suppose for a sliding window size of 3 a transition occurs from a dynamic component to a static component at time point t_o. When the entry of the sliding window is

at t_o, the component will be classified as dynamic, as it should be. Now, the window takes a step such that the exit of the sliding window is now at t_{o+1}. To check the component of motion the maximum displacement with in the window is calculated which will still lead to a dynamic component as the window includes displacements of the dynamic region (t_{o-1} and t_{o-2}). The next step that the window takes will still result in a dynamic component as the displacement of t_{o-1} will be included in the sliding window. Only, on the next step of the sliding window, where the entry of the sliding window is at t_o, will the component be classified as static. The question that arises from this example is which point should MixMAs consider as the point of transition, entry point of the sliding window or the exit point. In this case, the transition should be the point where the sliding window starts, and therefore the MixMAs program is designed to exactly that for dynamic to static transitions.

But, this static component will only be identified if the length of the static component is at least equal to the size of the sliding window. If the static component is 2 frames long (t_o to t_{o+2}), and a dynamic component follows it, then, when the sliding window start point is at t_o, its end will be at t_{o+3}. In this case the component will still be identified as dynamic. Thus, if a static component has a length less than the size of the sliding window MixMAs will miss it. This puts a limit to the length of identifiable static components equal to the size of the sliding window.

Example 2:

Consider the reverse case in which a transition occurs from a static component to a dynamic component at time point t_o. Still using a sliding window size of 3, when the exit of the sliding window is at t_o, the component will be classified as static as it should be. Now, the window takes a step such that the exit of the sliding window is now at t_{o+1}. To

check the component of motion the maximum displacement with in the window is calculated which will lead to a dynamic component be identified as the window includes 1 displacement of the dynamic region (t_{o+1}). In example 1, it was concluded that point of transition is at the entry point of the sliding window, which in this case if clearly wrong as the transition occurs at t_o and the entry of the sliding window at which MixMAs identifies the transition is t_{o-2}. In this case, the transition should be the point where the sliding window exits and therefore MixMAs is designed to do exactly that for static to dynamic transitions.

If the dynamic component is then followed by a static component, as in example 1, and the length of the dynamic component is less than the size of the sliding window then, in contrast to the missed brief static component in example 1, the brief dynamic component will still be identified. For example, if the length of the dynamic component occurring within an extended static state is two time intervals long followed by a transition back to a the extended static state, and if the window size is 3 time intervals, the window will contain a dynamic displacement for three steps.

In summary, dynamic regions with lengths less than the size of the sliding window will be successfully identified by MixMAs, whereas, static regions with lengths less than the size of the sliding window will be missed.

A pseudo-solution to this problem is using the smallest possible size of sliding window which is two time intervals (also the default size used by MixMAs). Another way in which this limitation of MixMAs can be overcome, is by increasing the rate at which the images are acquired. What this translates to is the following:

- Before (at a lower acquisition rate), the static events that were missed had a length lower that the size of the sliding window.

- By increasing the acquisition rate, the missed static region will now have a length that is greater than the size of the sliding window, therefore, it will not be missed.
- If, increasing the acquisition rate does not change the number of static events then, that means that no static events were being missed at the initial acquisition rate.

3.2.3. Other limitations

MixMAs currently analyzes 1-D and 2-D SPT data. It cannot currently analyze 3-D SPT data. However, this is not a limitation inherent to the algorithms used in the program, and future versions of MixMAs can be designed to include 3-D functionality.

Another limitation of MixMAs concerns the number of components it can recognize. In this study we have focused upon 3 components of motion; static, diffusive and directed. As a starting point for such a study this focus is sufficient and justified but one cannot ignore that motion can have some further sub-components. Also, one important parameter required for a complete description of directed motion (i-e., the direction of motion) cannot be determined by MixMAs. The following points highlight these 2 limitations:

In this study we have defined diffusive motion as a single component. MixMAs has been shown to identify diffusive components in a trajectory of a particle that has multiple components of motion and provide an alpha value and a step size for the diffusive motion. But a particle can have diffusive motion with 2 or more different diffusion coefficients, meaning it moves with a specific step size for a part of the diffusive motion but moves at significantly different step size for another part of the diffusive motion. In

this case, a particle has 2 sub-components within a diffusive component. A particle can have a number of such sub-components. MixMAs is limited in this regard, as it treats diffusive component as 1 single component and, therefore, in cases where a diffusive component has 2 or more sub-components, MixMAs's utility will be limited.

In this study we have defined directed motion and shown the capability of MixMAs to identify it in a trajectory for a particle that has multiple components of motion. But directed component also has a directionality associated with it. For example, a molecular motor can move towards the plus end of a microtubule or the minus end. MixMAs does not give any information regarding directionality and only provides an alpha value and a velocity value for the directed motion.

Lastly, MixMAs does not have the ability to perform brightness analysis. Due to this limitation, it assumes that all the particles in the data are single particles. Therefore, if complexes of particles are formed in an experiment, and their tracking information is included in the data input to MixMAs, these complexes will still be treated as single particles by MixMAs. The ability to perform brightness analysis can overcome this limitation as, MixMAs will then be able to distinguish single particles from complexes.

3.3 Future

3.3.1. Improvements

MixMAs uses a sliding window approach to identify transitions from one component of motion to another. As shown in the results section of chapter 2, this approach is suitable for particles that show motion with multi components. Another approach that has been used to tackle a similar problem is the 'Changepoint' approach (Heaslip et al., 2014). This approach is used to identify a single transition between diffusive and directed

components. In this approach a particle's trajectory is divided in to 2 parts. Then each part is fit to the diffusion equation and goodness of fit parameters (gofs) are calculated. These gofs are then used as variables for Bayesian Information Criterion (BIC) which gives a score as a result. The goal of the approach is to minimize the BIC score. To achieve this division of particle's trajectory, the division is performed at every time point and a BIC score is calculated. The time interval where the BIC score is minimum is classified as a transition point or a 'Changepoint'.

The advantage of this approach over the sliding window approach used in MixMAs is its accuracy in determining the point of transition. This is because, in sliding window analysis, when the sliding window spans the point of transition and classifies regions into different components, the identified transition point can have a maximum error that is equal to the size of the sliding window. Considering this fact, one can mistakenly conclude that the 'Changepoint' approach is better than the sliding window approach. But there is a major disadvantage to the 'Changepoint' approach. The 'Changepoint' approach only works for particles that only have a single transition point. This is because 'Changepoint' separates trajectories into 2 regions and if there is more than 1 transition the model fitting fails in the separated region where another transition is present as it was assumed that there is only 1 transition in the particle's trajectory. In contrast, as has been demonstrated, MixMAs succeeds even if there are 3 components of motion and all possible types of transitions take place between these 3 components.

The above discussion shows that both the approaches have their limitations and advantages. The above discussion also shows that if used together, the 2 approaches will complement each other nicely. MixMAs can be used to identify transition points first.

Then, based on the results 'Changepoint' can be used to separate trajectories within a few frames of the identified transition points and then, using the results from MixMAs about the components spanning the transition points fit the separated trajectories accordingly. An approach like this will increase accuracy of identification of transition points and will also work on trajectories with more than 2 components of motion and multiple transitions.

Another improvement that can be implemented in MixMAs is the ability of subtracting localization error from the displacement values. A point to consider here is that this can only be achieved if localization error has already been experimentally obtained. Apart from subtracting localization error, brightness analysis can also be incorporated into MixMAs. As already mentioned in the limitations section without this ability MixMAs is unable to distinguish between single particles and complexes of particles. With the incorporation of brightness analysis, MixMAs will be able to categorize particles into single particles and complexes. It will also be able further sub-categorize complexes based on the number of particles in those complexes.

3.4. Current study in a wider context: fluidity of lipid membranes

3.4.1. Membrane fluidity

Lipid bilayers form biological membranes such as cell membrane and membranes enclosing an organelle. The basic structure of a lipid bilayer is 2 layers of phospholipids with the hydrophilic phosphate containing heads exposed at the surfaces and the inner core composed of hydrophobic fatty acid chains.

In the structure described above the lipid bilayer is homogenous in which proteins can diffuse without any hinderance. But a biological membrane is more complex as it also has membrane proteins which are embedded in the lipid bilayer. These proteins also

interact with lipids and can also form protein complexes. Moreover, the fatty acid tails also differ in their composition; they can be saturated or unsaturated. Additionally, sterols are also imbedded in the membranes. The above-mentioned complexity results in a membrane that is not homogenous but has domains of different fluidity (also referred to as viscosity) (Pralle et al., 2000; Schutz et al., 2000). The study of membrane fluidity is crucial as it plays an important part in numerous physiological processes.

3.4.2. Physiological importance of regulating membrane fluidity

The physiological role of membrane fluidity is an area of active research. The evidence, so far, suggests that precise control of membrane fluidity is crucial for numerous cell processes, including protein sorting and trafficking in a cell, and cell signaling pathways. In protein trafficking pathway, membrane fluidity decreases from the start of the pathway in endoplasmic reticulum to the plasma membrane in a gradual manner. Evidence suggests that this gradient must be maintained for proper protein trafficking (Holthuis and Menon, 2014). Membrane fluidity also plays a crucial part in certain signaling cascades, such as receptor tyrosine kinase signaling pathways (Ge et al., 2001). In such signaling pathways, membrane sub-domains called ‘lipid rafts’ play an important role. Lipid rafts are subdomains of membranes which contain saturated phospholipids and cholesterol both of which decrease membrane fluidity and make these raft regions rigid. Receptors proteins can also be embedded in these rafts and in cases where an agonist needs to bind an activated receptor, these rafts, one containing the receptor protein and the other containing the activator protein, can coalesce allowing the agonist to bind the receptor and initiate its signaling cascade (Pralle et al., 2000; Ge et al., 2001).

Dysregulation of membrane fluidity has also been linked to the pathology of some diseases. For example, cardiolipin, which regulates mitochondrial membrane fluidity, dysfunction has been linked to Alzheimer's disease and traumatic brain injury. Although, whether cardiolipin's inability to regulate membrane fluidity is a part of the pathology of these diseases or not is still being researched (Zeczycki et al., 2014; Monteiro-Cardoso et al., 2015).

3.4.3. Determination of membrane fluidity using SPT in the context of current study

Over the years many techniques have been utilized to study membrane fluidity including Electron Paramagnetic Resonance, Fourier Transform Infrared Spectroscopy, Differential Scanning Calorimetry and fluorescence anisotropy. These techniques provided valuable information about membrane fluidity but were limited in the sense that they measured bulk fluidity of a membrane (Shinitzky et al., 1971; Lande et al., 1995; Subczynski et al., 2010; do Canto et al., 2016).

Although SPT analysis of *in vivo* membrane fluidity could in theory provide fluidity information about membrane sub-domains, its practical implementation was hindered by limitations in spatial resolution inherent to conventional light microscopy techniques.

With the advent of super resolution microscopy, it has become possible to achieve spatial resolutions of < 50nm. This advance in microscopy has led to numerous studies which have used SPT to study membrane fluidity *in vivo*, (Schutz et al., 2000; Eggeling et al., 2009; Sahl et al., 2010; Vicidomini et al., 2015) and the MixMAs analysis method is well suited for analysis of such data.

For example, in a membrane with distinct fluidity sub-regions, a particle can diffuse more freely where the membrane is relatively fluid, and less freely in regions with relatively lower fluidity such as lipid rafts. What this means is that such a dynamic particle will show motion with multiple components, just as do MAPs or molecular motor proteins. The algorithm defined in this study and used in MixMAs is thus applicable to the SPT data generated for such a particle.

This shows that there is a wide range of applicability of MixMAs; from analyzing SPT data of a molecular motor such as Kinesin-3 or a MAP such as Tau, to analyzing 2-D SPT data of a particle diffusing in a lipid membrane. It is hoped that availability of MixMAs will not only aid in the analysis of SPT data for molecular motors, MAPs and particles motion in a lipid membrane, but it will be useful for SPT data generated from a wide variety of studies from different areas of biology.

BIBLIOGRAPHY

Abboud R, Charcosset C, Greige-Gerges H (2018) Biophysical methods: Complementary tools to study the influence of human steroid hormones on the liposome membrane properties. Biochimie.

Adams SR, Campbell RE, Gross LA, Martin BR, Walkup GK, Yao Y, Llopis J, Tsien RY (2002) New biarsenical ligands and tetracysteine motifs for protein labeling in vitro and in vivo: synthesis and biological applications. J Am Chem Soc 124:6063-6076.

Aizawa H, Sekine Y, Takemura R, Zhang Z, Nangaku M, Hirokawa N (1992) Kinesin family in murine central nervous system. J Cell Biol 119:1287-1296.

Amos L, Klug A (1974) Arrangement of subunits in flagellar microtubules. J Cell Sci 14:523-549.

Amos LA, Baker TS (1979) The three-dimensional structure of tubulin protofilaments. Nature 279:607-612.

Amos LA, Schlieper D (2005) Microtubules and maps. Adv Protein Chem 71:257-298.

Andresen M, Schmitz-Salue R, Jakobs S (2004) Short tetracysteine tags to beta-tubulin demonstrate the significance of small labels for live cell imaging. Mol Biol Cell 15:5616-5622.

Baas PW, Deitch JS, Black MM, Banker GA (1988) Polarity orientation of microtubules in hippocampal neurons: uniformity in the axon and nonuniformity in the dendrite. Proc Natl Acad Sci U S A 85:8335-8339.

Barghorn S, Davies P, Mandelkow E (2004) Tau paired helical filaments from Alzheimer's disease brain and assembled in vitro are based on beta-structure in the core domain. Biochemistry 43:1694-1703.

Beese L, Stubbs G, Cohen C (1987) Microtubule structure at 18 A resolution. Journal of molecular biology 194:257-264.

Benke A, Olivier N, Gunzenhauser J, Manley S (2012) Multicolor single molecule tracking of stochastically active synthetic dyes. Nano Lett 12:2619-2624.

Betzig E, Patterson GH, Sougrat R, Lindwasser OW, Olenych S, Bonifacino JS, Davidson MW, Lippincott-Schwartz J, Hess HF (2006) Imaging intracellular fluorescent proteins at nanometer resolution. Science 313:1642-1645.

Brandt R, Hundelt M, Shahani N (2005) Tau alteration and neuronal degeneration in tauopathies: mechanisms and models. Biochimica et biophysica acta 1739.

Bunker J, Kamath K, Wilson L, Jordan M, Feinstein S (2006a) FTDP-17 Mutations Compromise the Ability of Tau to Regulate Microtubule Dynamics in Cells. The Journal of Biological Chemistry:11856-11863.

Bunker JM, Wilson L, Jordan MA, Feinstein SC (2004) Modulation of microtubule dynamics by tau in living cells: implications for development and neurodegeneration. Molecular biology of the cell 15.

Bunker JM, Kamath K, Wilson L, Jordan MA, Feinstein SC (2006b) FTDP-17 mutations compromise the ability of tau to regulate microtubule dynamics in cells. The Journal of biological chemistry 281.

Butner KA, Kirschner MW (1991) Tau protein binds to microtubules through a flexible array of distributed weak sites. The Journal of cell biology 115.

Campos C, Kamiya M, Banala S, Johnsson K, Gonzalez-Gaitan M (2011) Labelling cell structures and tracking cell lineage in zebrafish using SNAP-tag. Dev Dyn 240:820-827.

Cartelli D et al. (2016) alpha-Synuclein is a Novel Microtubule Dynamase. Sci Rep 6:33289.

Chaphalkar AR, Jain K, Gangan MS, Athale CA (2016) Automated Multi-Peak Tracking Kymography (AMTraK): A Tool to Quantify Sub-Cellular Dynamics with Sub-Pixel Accuracy. PLoS One 11:e0167620.

Chen CT, Doxsey SJ (2012) An MBoC favorite: role of GTP hydrolysis in microtubule dynamics: information from a slowly hydrolyzable analogue, GMPCPP. Mol Biol Cell 23:3775.

Chen I, Howarth M, Lin W, Ting AY (2005) Site-specific labeling of cell surface proteins with biophysical probes using biotin ligase. Nat Methods 2:99-104.

Connell JW, Gibb GM, Betts JC, Blackstock WP, Gallo J, Lovestone S, Hutton M, Anderton BH (2001) Effects of FTDP-17 mutations on the in vitro phosphorylation of tau by glycogen synthase kinase 3beta identified by mass spectrometry demonstrate certain mutations exert long-range conformational changes. FEBS Lett 493:40-44.

Cowan CM, Mudher A (2013) Are tau aggregates toxic or protective in tauopathies? Frontiers in neurology 4.

Dagenbach EM, Endow SA (2004) A new kinesin tree. J Cell Sci 117:3-7.

DeRocco V, Anderson T, Piehler J, Erie DA, Weninger K (2010) Four-color single-molecule fluorescence with noncovalent dye labeling to monitor dynamic multimolecular complexes. Biotechniques 49:807-816.

Dixit R, Ross JL, Goldman YE, Holzbaur EL (2008a) Differential regulation of dynein and kinesin motor proteins by tau. Science 319:1086-1089.

Dixit R, Ross JL, Goldman YE, Holzbaur EL (2008b) Differential regulation of dynein and kinesin motor proteins by tau. Science (New York, NY) 319.

do Canto A, Robalo JR, Santos PD, Carvalho AJP, Ramalho JPP, Loura LMS (2016) Diphenylhexatriene membrane probes DPH and TMA-DPH: A comparative molecular dynamics simulation study. Biochimica et biophysica acta 1858:2647-2661.

Drechsel DN, Hyman AA, Cobb MH, Kirschner MW (1992) Modulation of the dynamic instability of tubulin assembly by the microtubule-associated protein tau. Molecular biology of the cell 3.

Eggeling C, Ringemann C, Medda R, Schwarzmann G, Sandhoff K, Polyakova S, Belov VN, Hein B, von Middendorff C, Schonle A, Hell SW (2009) Direct observation of the nanoscale dynamics of membrane lipids in a living cell. Nature 457:1159-1162.

Esmaeli-Azad B, McCarty JH, Feinstein SC (1994) Sense and antisense transfection analysis of tau function: tau influences net microtubule assembly, neurite outgrowth and neuritic stability. Journal of cell science 107 (Pt 4).

Gardner MK, Zanic M, Howard J (2013) Microtubule catastrophe and rescue. Curr Opin Cell Biol 25:14-22.

Gatchel JR, Donovan NJ, Locascio JJ, Schultz AP, Becker JA, Chhatwal J, Papp KV, Amariglio RE, Rentz DM, Blacker D, Sperling RA, Johnson KA, Marshall GA (2017) Depressive Symptoms and Tau Accumulation in the Inferior Temporal Lobe and Entorhinal Cortex in Cognitively Normal Older Adults: A Pilot Study. J Alzheimers Dis 59:975-985.

Gauthier-Kemper A, Weissmann C, Golovyashkina N, Sebo-Lemke Z, Drewes G, Gerke V, Heinisch JJ, Brandt R (2011) The frontotemporal dementia mutation R406W blocks tau's interaction with the membrane in an annexin A2-dependent manner. J Cell Biol 192:647-661.

Ge G, Wu J, Lin Q (2001) Effect of membrane fluidity on tyrosine kinase activity of reconstituted epidermal growth factor receptor. Biochem Biophys Res Commun 282:511-514.

Goedert M, Jakes R (1990) Expression of separate isoforms of human tau protein: correlation with the tau pattern in brain and effects on tubulin polymerization. The EMBO journal 9.

Goedert M, Crowther RA, Spillantini MG (1998) Tau mutations cause frontotemporal dementias. Neuron 21:955-958.

Goode BL, Feinstein SC (1994) Identification of a novel microtubule binding and assembly domain in the developmentally regulated inter-repeat region of tau. The Journal of cell biology 124.

Goode BL, Chau M, Denis PE, Feinstein SC (2000) Structural and functional differences between 3-repeat and 4-repeat tau isoforms. Implications for normal tau function and the onset of neurodegenetative disease. The Journal of biological chemistry 275.

Gustafsson MG (2000) Surpassing the lateral resolution limit by a factor of two using structured illumination microscopy. Journal of microscopy 198:82-87.

Gustke N, Trinczek B, Biernat J, Mandelkow EM, Mandelkow E (1994) Domains of tau protein and interactions with microtubules. Biochemistry 33.

Heaslip AT, Nelson SR, Lombardo AT, Beck Previs S, Armstrong J, Warshaw DM (2014) Cytoskeletal dependence of insulin granule movement dynamics in INS-1 beta-cells in response to glucose. PLoS One 9:e109082.

Henderson R, Unwin PN (1975) Three-dimensional model of purple membrane obtained by electron microscopy. Nature 257:28-32.

Henriques AG, Vieira SI, da Cruz ESEF, da Cruz ESOA (2010) Abeta promotes Alzheimer's disease-like cytoskeleton abnormalities with consequences to APP processing in neurons. J Neurochem 113:761-771.

Hinrichs MH, Jalal A, Brenner B, Mandelkow E, Kumar S, Scholz T (2012) Tau protein diffuses along the microtubule lattice. The Journal of biological chemistry 287.

Hirokawa N (1998) Kinesin and dynein superfamily proteins and the mechanism of organelle transport. Science 279:519-526.

Hirokawa N, Pfister KK, Yorifuji H, Wagner MC, Brady ST, Bloom GS (1989) Submolecular domains of bovine brain kinesin identified by electron microscopy and monoclonal antibody decoration. Cell 56:867-878.

Holthuis JC, Menon AK (2014) Lipid landscapes and pipelines in membrane homeostasis. Nature 510:48-57.

Hyman AA, Salser S, Drechsel DN, Unwin N, Mitchison TJ (1992) Role of GTP hydrolysis in microtubule dynamics: information from a slowly hydrolyzable analogue, GMPCPP. Mol Biol Cell 3:1155-1167.

Iyer A, LaPointe N, Zielke K, Berdynski M, Guzman E, Barczak A, Zebrowska M, Barcikowska M, Feinstein S, C Z (2013) A Novel MAPT Mutation, G55R, in a Frontotemporal Dementia Patient Leads to Altered Tau Function. PLOS one.

Jaqaman K, Loerke D, Mettlen M, Kuwata H, Grinstein S, Schmid SL, Danuser G (2008) Robust single-particle tracking in live-cell time-lapse sequences. Nat Methods 5:695-702.

Jones WC (1975) The pattern of microtubules in the axonemes of Gymnosphaera albida sassaki: evidence for 13 protofilaments. J Cell Sci 18:135-155.

Kandel ER, Schwartz, J. H., and Jessell, T. M. (1995) Nerve cells and behavior. In: In Essentials of neuroscience and behavior, pp 21-31. Norwalk: Appleton & Lange.

Kellner RR, Baier CJ, Willig KI, Hell SW, Barrantes FJ (2007) Nanoscale organization of nicotinic acetylcholine receptors revealed by stimulated emission depletion microscopy. Neuroscience 144:135-143.

Kempf M, Clement A, Faissner A, Lee G, Brandt R (1996) Tau binds to the distal axon early in development of polarity in a microtubule- and microfilament-dependent manner. J Neurosci 16:5583-5592.

Kerssemakers JW, Munteanu EL, Laan L, Noetzel TL, Janson ME, Dogterom M (2006) Assembly dynamics of microtubules at molecular resolution. Nature 442:709-712.

Konzack S, Thies E, Marx A, Mandelkow EM, Mandelkow E (2007) Swimming against the tide: mobility of the microtubule-associated protein tau in neurons. The Journal of neuroscience : the official journal of the Society for Neuroscience 27.

Lande MB, Donovan JM, Zeidel ML (1995) The relationship between membrane fluidity and permeabilities to water, solutes, ammonia, and protons. The Journal of general physiology 106:67-84.

Lawrence CJ et al. (2004) A standardized kinesin nomenclature. J Cell Biol 167:19-22.

LeBoeuf A, Levy S, Gaylord M, Bhattacharya A, Singh A, Jordan M, Wilson L, Feinstein S (2008a) FTDP-17 Mutations in Tau Alter the Regulation of Microtubule Dynamics; AN "ALTERNATE CORE" MODEL FOR NORMAL AND PATHOLOGICAL TAU ACTION. The Journal Of Biological Chemistry:36406-36415.

LeBoeuf AC, Levy SF, Gaylord M, Bhattacharya A, Singh AK, Jordan MA, Wilson L, Feinstein SC (2008b) FTDP-17 mutations in Tau alter the regulation of microtubule dynamics: an "alternative core" model for normal and pathological Tau action. The Journal of biological chemistry 283.

Levy SF, LeBoeuf AC, Massie MR, Jordan MA, Wilson L, Feinstein SC (2005) Three- and four-repeat tau regulate the dynamic instability of two distinct microtubule subpopulations in qualitatively different manners. Implications for neurodegeneration. The Journal of biological chemistry 280.

Li C, Li J, Goodson HV, Alber MS (2014) Microtubule dynamic instability: the role of cracks between protofilaments. Soft Matter 10:2069-2080.

Liu SL, Li J, Zhang ZL, Wang ZG, Tian ZQ, Wang GP, Pang DW (2013) Fast and high-accuracy localization for three-dimensional single-particle tracking. Sci Rep 3:2462.

Lodish H BA, Zipursky SL, Matsudaira P, Baltimore D, Darnell EJ. (2000) Overview of Neuron Structure and Function. In: Molecular Cell Biology, 4th Edition. New York: W.H. Freeman & Company.

Maday S, Twelvetrees AE, Moughamian AJ, Holzbaur EL (2014) Axonal transport: cargo-specific mechanisms of motility and regulation. Neuron 84:292-309.

Mandelkow EM, Stamer K, Vogel R, Thies E, Mandelkow E (2003) Clogging of axons by tau, inhibition of axonal traffic and starvation of synapses. Neurobiology of aging 24.

Mandelkow EM, Biernat J, Drewes G, Gustke N, Trinczek B, Mandelkow E (1995) Tau domains, phosphorylation, and interactions with microtubules. Neurobiology of aging 16.

Mangeol P, Prevo B, Peterman EJ (2016) KymographClear and KymographDirect: two tools for the automated quantitative analysis of molecular and cellular dynamics using kymographs. Mol Biol Cell 27:1948-1957.

McVicker DP, Chrin LR, Berger CL (2011a) The nucleotide-binding state of microtubules modulates kinesin processivity and the ability of Tau to inhibit kinesin-mediated transport. J Biol Chem 286:42873-42880.

McVicker DP, Chrin LR, Berger CL (2011b) The nucleotide-binding state of microtubules modulates kinesin processivity and the ability of Tau to inhibit kinesin-mediated transport. The Journal of biological chemistry 286.

McVicker DP, Hoeprich GJ, Thompson AR, Berger CL (2014) Tau interconverts between diffusive and stable populations on the microtubule surface in an isoform and lattice specific manner. Cytoskeleton (Hoboken, NJ) 71.

Mercken M, Fischer I, Kosik KS, Nixon RA (1995) Three distinct axonal transport rates for tau, tubulin, and other microtubule-associated proteins: evidence for dynamic interactions of tau with microtubules in vivo. The Journal of neuroscience : the official journal of the Society for Neuroscience 15.

Mitchison T, Kirschner M (1984) Dynamic instability of microtubule growth. Nature 312:237-242.

Monteiro-Cardoso VF, Oliveira MM, Melo T, Domingues MR, Moreira PI, Ferreiro E, Peixoto F, Videira RA (2015) Cardiolipin profile changes are associated to the early

synaptic mitochondrial dysfunction in Alzheimer's disease. J Alzheimers Dis 43:1375-1392.

Mukrasch MD, von Bergen M, Biernat J, Fischer D, Griesinger C, Mandelkow E, Zweckstetter M (2007) The "jaws" of the tau-microtubule interaction. The Journal of biological chemistry 282.

Nogales E, Whittaker M, Milligan RA, Downing KH (1999) High-resolution model of the microtubule. Cell 96:79-88.

Oakley BR, Paolillo V, Zheng Y (2015) gamma-Tubulin complexes in microtubule nucleation and beyond. Mol Biol Cell 26:2957-2962.

Okada Y, Hirokawa N (2000) Mechanism of the single-headed processivity: diffusional anchoring between the K-loop of kinesin and the C terminus of tubulin. Proc Natl Acad Sci U S A 97:640-645.

Okada Y, Yamazaki H, Sekine-Aizawa Y, Hirokawa N (1995) The neuron-specific kinesin superfamily protein KIF1A is a unique monomeric motor for anterograde axonal transport of synaptic vesicle precursors. Cell 81:769-780.

Panda D, Goode BL, Feinstein SC, Wilson L (1995) Kinetic stabilization of microtubule dynamics at steady state by tau and microtubule-binding domains of tau. Biochemistry 34.

Panda D, Samuel JC, Massie M, Feinstein SC, Wilson L (2003) Differential regulation of microtubule dynamics by three- and four-repeat tau: implications for the onset of neurodegenerative disease. Proceedings of the National Academy of Sciences of the United States of America 100.

Pierce DW, Vale RD (1999) Single-molecule fluorescence detection of green fluorescence protein and application to single-protein dynamics. Methods Cell Biol 58:49-73.

Pralle A, Keller P, Florin EL, Simons K, Horber JK (2000) Sphingolipid-cholesterol rafts diffuse as small entities in the plasma membrane of mammalian cells. J Cell Biol 148:997-1008.

Preuss U, Biernat J, Mandelkow EM, Mandelkow E (1997) The 'jaws' model of tau-microtubule interaction examined in CHO cells. Journal of cell science 110 (Pt 6).

Raeisolsadati Oskouei M, Brouwer AM (2017) Organocatalytic Fluorogenic Synthesis of Chromenes. J Fluoresc 27:1141-1147.

Ram S, Prabhat P, Chao J, Ward ES, Ober RJ (2008) High accuracy 3D quantum dot tracking with multifocal plane microscopy for the study of fast intracellular dynamics in live cells. Biophysical journal 95:6025-6043.

Reece JB, Urry, L. A., Cain, M. L., Wasserman, S. A., Minorsky, P. V., and Jackson, R. B. (2011) Nervous systems consist of circuits of neurons and supporting cells. In: Campbell Biology, 10th Edition, pp 1080-1084. San Francisco: Pearson.

Rice S, Lin AW, Safer D, Hart CL, Naber N, Carragher BO, Cain SM, Pechatnikova E, Wilson-Kubalek EM, Whittaker M, Pate E, Cooke R, Taylor EW, Milligan RA, Vale RD (1999) A structural change in the kinesin motor protein that drives motility. Nature 402:778-784.

Ruhnow F, Zwicker D, Diez S (2011) Tracking single particles and elongated filaments with nanometer precision. Biophysical journal 100:2820-2828.

Ruschel J, Hellal F, Flynn KC, Dupraz S, Elliott DA, Tedeschi A, Bates M, Sliwinski C, Brook G, Dobrindt K, Peitz M, Brustle O, Norenberg MD, Blesch A, Weidner N, Bunge MB, Bixby JL, Bradke F (2015) Axonal regeneration. Systemic administration of epothilone B promotes axon regeneration after spinal cord injury. Science 348:347-352.

Sage D, Neumann FR, Hediger F, Gasser SM, Unser M (2005) Automatic tracking of individual fluorescence particles: application to the study of chromosome dynamics. IEEE transactions on image processing : a publication of the IEEE Signal Processing Society 14:1372-1383.

Sahl SJ, Leutenegger M, Hilbert M, Hell SW, Eggeling C (2010) Fast molecular tracking maps nanoscale dynamics of plasma membrane lipids. Proc Natl Acad Sci U S A 107:6829-6834.

Samsonov A, Yu JZ, Rasenick M, Popov SV (2004) Tau interaction with microtubules in vivo. Journal of cell science 117.

Schermelleh L, Carlton PM, Haase S, Shao L, Winoto L, Kner P, Burke B, Cardoso MC, Agard DA, Gustafsson MG, Leonhardt H, Sedat JW (2008) Subdiffraction multicolor imaging of the nuclear periphery with 3D structured illumination microscopy. Science 320:1332-1336.

Schmoranzer J, Goulian M, Axelrod D, Simon SM (2000) Imaging constitutive exocytosis with total internal reflection fluorescence microscopy. J Cell Biol 149:23-32.

Schnapp BJ, Reese TS (1989) Dynein is the motor for retrograde axonal transport of organelles. Proc Natl Acad Sci U S A 86:1548-1552.

Schutz GJ, Kada G, Pastushenko VP, Schindler H (2000) Properties of lipid microdomains in a muscle cell membrane visualized by single molecule microscopy. The EMBO Journal 19:892-901.

Seitz A, Kojima H, Oiwa K, Mandelkow EM, Song YH, Mandelkow E (2002) Single-molecule investigation of the interference between kinesin, tau and MAP2c. The EMBO journal 21.

Shank NI, Pham HH, Waggoner AS, Armitage BA (2013) Twisted cyanines: a non-planar fluorogenic dye with superior photostability and its use in a protein-based fluoromodule. J Am Chem Soc 135:242-251.

Shinitzky M, Dianoux AC, Gitler C, Weber G (1971) Microviscosity and order in the hydrocarbon region of micelles and membranes determined with fluorescent probes. I. Synthetic micelles. Biochemistry 10:2106-2113.

Smith R, Bacos K, Fedele V, Soulet D, Walz HA, Obermuller S, Lindqvist A, Bjorkqvist M, Klein P, Onnerfjord P, Brundin P, Mulder H, Li JY (2009) Mutant huntingtin interacts with {beta}-tubulin and disrupts vesicular transport and insulin secretion. Hum Mol Genet 18:3942-3954.

Song Y, DiMaio F, Wang RY, Kim D, Miles C, Brunette T, Thompson J, Baker D (2013) High-resolution comparative modeling with RosettaCM. Structure 21:1735-1742.

Stamer K, Vogel R, Thies E, Mandelkow E, Mandelkow EM (2002) Tau blocks traffic of organelles, neurofilaments, and APP vesicles in neurons and enhances oxidative stress. The Journal of cell biology 156.

Stern JL, Lessard DV, Hoeprich GJ, Morfini GA, Berger CL (2017) Phosphoregulation of Tau modulates inhibition of kinesin-1 motility. Mol Biol Cell 28:1079-1087.

Stewart RJ, Farrell KW, Wilson L (1990) Role of GTP hydrolysis in microtubule polymerization: evidence for a coupled hydrolysis mechanism. Biochemistry 29:6489-6498.

Stoothoff W, Jones PB, Spires-Jones TL, Joyner D, Chhabra E, Bercury K, Fan Z, Xie H, Bacskai B, Edd J, Irimia D, Hyman BT (2009a) Differential effect of three-repeat and four-repeat tau on mitochondrial axonal transport. J Neurochem 111:417-427.

Stoothoff W, Jones PB, Spires-Jones TL, Joyner D, Chhabra E, Bercury K, Fan Z, Xie H, Bacskai B, Edd J, Irimia D, Hyman BT (2009b) Differential effect of three-repeat and four-repeat tau on mitochondrial axonal transport. Journal of neurochemistry 111.

Subczynski WK, Raguz M, Widomska J (2010) Studying lipid organization in biological membranes using liposomes and EPR spin labeling. Methods in molecular biology (Clifton, NJ) 606:247-269.

Sulimenko V, Hajkova Z, Klebanovych A, Draber P (2017) Regulation of microtubule nucleation mediated by gamma-tubulin complexes. Protoplasma 254:1187-1199.

Svoboda K, Schmidt CF, Schnapp BJ, Block SM (1993) Direct observation of kinesin stepping by optical trapping interferometry. Nature 365:721-727.

Thompson NL, Lagerholm BC (1997) Total internal reflection fluorescence: applications in cellular biophysics. Current opinion in biotechnology 8:58-64.

Tilney LG, Bryan J, Bush DJ, Fujiwara K, Mooseker MS, Murphy DB, Snyder DH (1973) Microtubules: evidence for 13 protofilaments. J Cell Biol 59:267-275.

Toomre D, Manstein DJ (2001) Lighting up the cell surface with evanescent wave microscopy. Trends in cell biology 11:298-303.

Trinczek B, Ebneth A, Mandelkow EM, Mandelkow E (1999) Tau regulates the attachment/detachment but not the speed of motors in microtubule-dependent transport of single vesicles and organelles. Journal of cell science 112 (Pt 14).

Trinczek B, Biernat J, Baumann K, Mandelkow EM, Mandelkow E (1995) Domains of tau protein, differential phosphorylation, and dynamic instability of microtubules. Molecular biology of the cell 6.

Vale RD, Reese TS, Sheetz MP (1985) Identification of a novel force-generating protein, kinesin, involved in microtubule-based motility. Cell 42:39-50.

Vershinin M, Carter BC, Razafsky DS, King SJ, Gross SP (2007) Multiple-motor based transport and its regulation by Tau. Proceedings of the National Academy of Sciences of the United States of America 104.

Vershinin M, Xu J, Razafsky DS, King SJ, Gross SP (2008) Tuning microtubule-based transport through filamentous MAPs: the problem of dynein. Traffic (Copenhagen, Denmark) 9.

Vicidomini G, Ta H, Honigmann A, Mueller V, Clausen MP, Waithe D, Galiani S, Sezgin E, Diaspro A, Hell SW, Eggeling C (2015) STED-FLCS: An Advanced Tool to Reveal Spatiotemporal Heterogeneity of Molecular Membrane Dynamics. Nano Lett 15:5912-5918.

Walker RA, O'Brien ET, Pryer NK, Soboeiro MF, Voter WA, Erickson HP, Salmon ED (1988) Dynamic instability of individual microtubules analyzed by video light microscopy: rate constants and transition frequencies. J Cell Biol 107:1437-1448.

Wang JZ, Xia YY, Grundke-Iqbal I, Iqbal K (2013) Abnormal hyperphosphorylation of tau: sites, regulation, and molecular mechanism of neurofibrillary degeneration. Journal of Alzheimer's disease : JAD 33 Suppl 1.

Weingarten MD, Lockwood AH, Hwo SY, Kirschner MW (1975) A protein factor essential for microtubule assembly. Proceedings of the National Academy of Sciences of the United States of America 72.

Willig KI, Harke B, Medda R, Hell SW (2007) STED microscopy with continuous wave beams. Nat Methods 4:915-918.

Willig KI, Rizzoli SO, Westphal V, Jahn R, Hell SW (2006a) STED microscopy reveals that synaptotagmin remains clustered after synaptic vesicle exocytosis. Nature 440:935-939.

Willig KI, Kellner RR, Medda R, Hein B, Jakobs S, Hell SW (2006b) Nanoscale resolution in GFP-based microscopy. Nat Methods 3:721-723.

Witman GB, Cleveland DW, Weingarten MD, Kirschner MW (1976) Tubulin requires tau for growth onto microtubule initiating sites. Proceedings of the National Academy of Sciences of the United States of America 73.

Xiao X, Geyer VF, Bowne-Anderson H, Howard J, Sbalzarini IF (2016) Automatic optimal filament segmentation with sub-pixel accuracy using generalized linear models and B-spline level-sets. Med Image Anal 32:157-172.

Yang JT, Laymon RA, Goldstein LS (1989) A three-domain structure of kinesin heavy chain revealed by DNA sequence and microtubule binding analyses. Cell 56:879-889.

Zeczycki TN, Whelan J, Hayden WT, Brown DA, Shaikh SR (2014) Increasing levels of cardiolipin differentially influence packing of phospholipids found in the mitochondrial inner membrane. Biochem Biophys Res Commun 450:366-371.

Zheng Y, Wong ML, Alberts B, Mitchison T (1995) Nucleation of microtubule assembly by a gamma-tubulin-containing ring complex. Nature 378:578-583.

APPENDIX

The following points are intended to aid users in the interpretation of the results obtained from MixMAs. Additionally, a few suggestions are also given which will improve the accuracy of MixMAs, and therefore increase the confidence of users on the obtained results.

- Although not required, it is suggested that the users know the number and the types of motion components their particle of interest exhibits. This knowledge can be obtained from a preliminary analysis of the data. Such analysis can be based on a visual inspection of a few kymographs or a visual inspection of a few displacement vs. time graphs. As an example, kymographs for Tau show that it has diffusive and static components only, whereas kymographs for Kinesin-3 show that it has all three components of motion. So, for Tau, the direction cutoff can be safely set to 0 and for Kinesin-3 it can be determined by MixMAs.
- MixMAs assumes that all the particles are of a single type. By this, I mean that all the particles are either monomers or dimers or complexes etc. The reason for this assumption is that brightness analysis of particles is not incorporated into MixMAs. If possible, brightness analysis should be performed before analyzing data using MixMAs. Another way in which the probability of tracking single particles can be increased is by using a relatively low concentration of labelled particles, thereby decreasing the probability of particles forming complexes.
- The cutoffs generated by MixMAs rely on two variables: an estimate of the localization error and an estimate of the particle step size. A suggestion for increasing the accuracy of MixMAs is to determine the localization error

experimentally rather than estimating it. This can be achieved by fixing the particle of interest to a glass slide or a coverslip (or any other way that ensures that the particle is static) and then tracking its motion. The mean of the displacements obtained from the tracking data will yield a better estimate of localization error and therefore improve the accuracy of MixMAs.

- The algorithm used in MixMAs has an inherent limitation: if a static component's length is less than the size of the sliding window, then that component is missed. A possible solution to overcoming this limitation is to increase the rate at which images are acquired. If the results obtained from MixMAs do not change then the user can be confident that no static events are missed. If, there is an increase in the number of static events then the image acquisition rate should be increased further until the results do not change. One problem that arises by increasing the image acquisition rate is that the probability of photobleaching increases. Therefore, if such a case arises, then this inherent limitation of MixMAs should be considered when interpreting the results obtained from analysis with MixMAs.